Scholar Commons
USF University of South Florida

University of South Florida
Scholar Commons

Graduate Theses and Dissertations | Graduate School

June 2018

Simulation of Turbulent Air Jet Impingement for Commercial Cooking Applications

Shantanu S. Shevade
University of South Florida, sshevade@mail.usf.edu

Follow this and additional works at: https://scholarcommons.usf.edu/etd

 Part of the Mechanical Engineering Commons

Scholar Commons Citation

Shevade, Shantanu S., "Simulation of Turbulent Air Jet Impingement for Commercial Cooking Applications" (2018). *Graduate Theses and Dissertations.*
https://scholarcommons.usf.edu/etd/7362

This Dissertation is brought to you for free and open access by the Graduate School at Scholar Commons. It has been accepted for inclusion in Graduate Theses and Dissertations by an authorized administrator of Scholar Commons. For more information, please contact scholarcommons@usf.edu.

Simulation of Turbulent Air Jet Impingement for Commercial Cooking Applications

by

Shantanu S. Shevade

A dissertation submitted in partial fulfillment
of the requirements for the degree of
Doctor of Philosophy in Mechanical Engineering
Department of Mechanical Engineering
College of Engineering
University of South Florida

Co-Major Professor: Rasim Guldiken, Ph.D.
Co-Major Professor: Muhammad Rahman, Ph.D.
Frank Pyrtle III, Ph.D.
Sanjukta Bhanja, Ph.D.
Yuncheng You, Ph.D.

Date of Approval:
June 6, 2018

Keywords: Heat Transfer, Nozzles, Air Flow, Parametric Analysis, Oven

Copyright © 2018, Shantanu S. Shevade

DEDICATION

I would like to dedicate this work to my parents Sudhir and Maitreyee Shevade, who instilled the importance of higher education in me since my childhood. I wouldn't be here today if it wasn't for you to allow me to pursue my dreams. Thank you for the sacrifices you have made for betterment of our family.

To my kids Meera, Cyrus and Selena, who gave me the reason to push forward. I hope to be an inspiration to you in your quest to pursue higher studies. To my wife, Vibha, who removed roadblocks to allow me to dedicate my time towards completion of my doctoral degree. Thank you for always pushing me to finish what I had started.

To Sudhanshu and Dr. Gauri, for being one of the nicest brother and sister-in-law, I could ever ask for and to my in-laws late Dr. Devindra Dhawan and late Promila Dhawan for believing in me. This work is dedicated to all of you.

ACKNOWLEDGMENTS

I would like to acknowledge key people who have been instrumental during my time as a doctoral student.

Dr. Guldiken, you accepted me in the program and never questioned my ability to complete the work. You have been a source of constant energy which fueled my pursuit for Ph.D. I felt a new wave of enthusiasm after every meeting that you and I had over the past several months. It pushed me to get to where I am today.

Dr. Rahman, words cannot express how grateful I am to you. I have been with you since I started as a student at USF and you never lost faith in me through the times when I wasn't able to focus on my education. Over the many publications we worked on together, I learned a lot from you through your attention to detail and pursuit of excellence.

I firmly believe that I wouldn't be here to the point of writing this acknowledgement if it wasn't for both of your support. Thank you very much from the bottom of my heart. I hope we will keep working together on exciting new publications in future.

Dr. Sanjukta Bhanja, Dr. Frank Pyrtle III and Dr. Yuncheng You, my committee members, and Dr. Andres Tejada-Martinez, my committee chair, thank you for your time and effort to review my work. I am grateful for the support you have given me to allow me to complete my doctoral degree.

Thank you, Kenneth Lundberg for providing me tools to complete this work. Thank you to my friends John Daly, Hari Patel & Parthiv Patel for keeping my brain energized with all the

intellectual conversations we had over the years. Yaricet Ruiz, thank you for doing all the complicated paperwork so I could restart my program in Fall 2016. The whole process seemed like a breeze because of your immense help.

Without each one of you, this would not have been possible.

TABLE OF CONTENTS

LIST OF TABLES

LIST OF FIGURES

ABSTRACT

The research work in this dissertation focuses on turbulent air jet heat transfer for commercial cooking applications.

As a part of this study, convective heat transfer coefficient and its interdependency with various key parameters is analyzed for single nozzle turbulent jet impingement. Air is used as the working fluid impinging on the flat surface. A thorough investigation of velocity and temperature distributions is performed by varying nozzle velocity and height over diameter ratio (H/D). Nusselt number and Turbulent Energy are presented for the impingement surface. It was found that for H/D ratios ranging between 6 and 8, nozzle velocities over 20 m/s provide a large percentage increase in heat transfer.

Single nozzle jet impingement is followed by study of turbulent multi-jet impingement. Along with parameters mentioned above, spacing over diameter ratio (S/D) is varied. Convective heat transfer coefficient, average impingement surface temperature and heat transfer rate are calculated over the impingement surface. It was found that higher S/D ratios result in higher local heat transfer coefficient values near stagnation point. However, increased spacing between the neighboring jets results in reduced coverage of the impingement surface lowering the average heat transfer. Lower H/D ratios result in higher heat transfer coefficient peaks. The peaks for all three nozzles are more uniform for H/D ratios between 6 and 8. For a fixed nozzle velocity, heat transfer coefficient values are directly proportional to nozzle diameter. For a fixed H/D and S/D ratio, heat transfer rate and average impingement surface temperature increases as the nozzle

velocity increases until it reaches a limiting value. Further increase in nozzle velocity causes drop in heat transfer rate due to ingress of large amounts of cold ambient air in the control volume.

The final part of this dissertation focuses on case study of conveyor oven. Lessons learned from analysis of single and multi-jet impingement are implemented in the case study. A systematic approach is used to arrive to an optimal configuration of the oven. As compared to starting configuration, for optimized configuration the improvement in average heat transfer coefficient was 22.7%, improvement in average surface heat flux was 24.7% and improvement in leakage air mass flow rate was 59.1%.

CHAPTER 1: INTRODUCTION

Commercial foodservice industry is evolving at a rapid pace. Along with the need to continuously improve equipment performance, industry is looking at innovative ways to prepare, cook and store food. Lowering energy consumption and maintaining higher quality standards for food dictates cooking food efficiently and faster than ever before while preserving its essential taste. Cooking and storing food at elevated temperatures with forced air is one of the most efficient ways to meet the demands of the industry. Heat transfer coefficients in cooking food with impinged air have known to reach values in the range of 150 W/m^2K - 250 W/m^2K as compared to under 100 W/m^2K using traditional approaches. To further improve heat transfer, a deep understanding of how jet impingement works, is essential. By analyzing and studying air impingement, performance improvement in foodservice equipment can be achieved. In this research, Computational Fluid Dynamics (CFD) simulation is used to analyze turbulent jet impingement by varying key parameters. To validate model, the simulation is verified against known experimental results. The simulation is further improved by analyzing interdependencies between different variables such as nozzle velocities, H/D ratio and S/D ratio.

1.1 Motivation for this Research

Cooking food with high temperature jet impingement is becoming more and more popular. As consumers expect quicker speed of service while maintaining the quality of food, hot air jet impingement is finding its application in cooking a wide variety of food products. Organizations involved in development of foodservice equipment have relied on traditional

methods for development and testing of new equipment. This involves fabricating a large number of physical parts that can be assembled in different configurations and using hundreds of measurement instruments and sensors to successfully test the equipment. This not only lengthens the development timeline but also increases the possibility of human error during testing. Advances in simulation software and powerful computing machines have presented a unique opportunity to accurately simulate fluid flows in foodservice sector while dramatically reducing computational times. These strengths can be leveraged against the traditional approaches resulting in reduced development times for foodservice equipment. There can be no substitute for an actual field test but using simulation early in development stage reduces the total sample size required to get to an optimum configuration. The post processing capabilities of simulation software also helps engineers to visualize the flow field. This greatly helps in solving existing problems and implement product improvements. This can directly affect the quality of food we consume at home or in restaurants. Capitalizing on the tools that are available to us to improve foodservice equipments thereby improving quality of food is the primary motivation behind this research.

1.2 Dissertation Structure

The research work is divided into following chapters.

In chapter two literature search is carried out on existing published material. Papers involving single and multiple air jet impingement are discussed. Publications involved in applications such as ovens are also listed. The aim is to lay out the background work while pointing out the uniqueness of this research.

In chapter three, jet impingement by a single un-bound jet on a flat plate is analyzed. Model is validated against prior literature. Heat transfer coefficients are studied by varying

various parameters such as nozzle velocity, nozzle diameter and distance between impingement surface and nozzle. Important relation between stagnation zone and nozzle diameter is discovered. Effect of different nozzle velocities on boundary layer thickness is studied.

In chapter four, jet impingement by three nozzle arrangements is studied. With multiple nozzles, interaction between neighboring nozzles becomes an important factor in overall heat transfer. This interaction is studied in depth coupled with flow trajectories as well as velocity and temperature cut plots to give a visual representation of flow patterns. Interesting observations are made regarding reverse flow between the jets and its effect on heat transfer. Number of key parameters are varied to understand their influence on effectivity of multiple jets.

Lessons learned from chapter three and four are applied to a real-world problem in chapter five. Thermally balancing and optimizing performance of conveyor ovens is a complicated problem requiring thorough understanding of multiple turbulent air jet impingement. A 3D model of a conveyor oven is created. Number of high impact parameters are varied through a systematic approach. Velocity distribution and air leakage from the oven to surrounding air is analyzed. Surface heat flux and heat transfer coefficient is studied. Through process of optimization, an oven configuration is selected which is expected to perform ~20% better than the starting configuration.

This research explores the jet impingement problem from analytical point of view but author's experience in foodservice environment and manufacturing industry is used to ensure analysis is grounded in real-world practices.

1.3 Nomenclature

C_p Constant pressure specific heat, J/kgK

D Diameter of nozzle, m

D_h Hydraulic diameter, m

h Heat transfer coefficient, $q_{int}/(T_{int}-T_b)$

H Height of computational domain, m

k Thermal conductivity, W/mK; or Turbulent kinetic energy, m^2/s^2

L Length of computational domain, m

Nu Nusselt number, hD_h/k_f

p Pressure, N/m^2

Pr_t Turbulent Prandtl number

q Heat flux, W/m^2

Re Reynolds number, $\rho_f w_{in} D_h/\mu$

t Time, s

T Temperature, ^0C

ΔT Inlet and outlet temperature difference, ^0C

u Velocity in x-direction, m/s

v Velocity in y-direction, m/s

V Velocity, m/s

w Velocity in z-direction, m/s

W Width of computational domain, m

Greek symbols

α Thermal diffusivity, m^2/s

Δ Displacement, m

ε Dissipation rate of turbulent kinetic energy, m^2/s^3

ν Kinematic viscosity, m^2/s

ν_t Turbulent viscosity, m^2/s

ρ Density, kg/m^3

Subscripts

amb Ambient

b Bulk

f Fluid

in Inlet

int Interface

max Maximum

noz Nozzle

s Solid

CHAPTER 2: LITERATURE REVIEW

In this chapter literature review is conducted on existing literature related to air jet impingement. Published papers related to single and multiple air jet impingement are studied.

Erdogdu et al. studied air-impingement cooling process for boiled eggs [1]. The model was built in a CFD software and validated against experimental data such as particle image velocimetry -PIV data and temperature data. Different cooling conditions were simulated to show effectiveness of air-impingement system. The researchers mentioned the need to further analyze this process by varying H/D ratios, nozzle arrangements and effects of higher Reynolds number.

Anderson and Singh conducted experiments to obtain heat transfer coefficient during thawing [2]. Heat transfer coefficients and its relation to location was determined. It was found that heat transfer coefficient increased with time. Along the radial length, heat transfer coefficients decreased. At a distance equal to nozzle diameter, secondary peaks were observed.

Experimental study on circular jet impinging on flat plate was conducted by Guo et al. [3]. Heat transfer parameters were obtained. With nozzle diameter of 6 mm, Reynolds number was varied from ~10K – 50K. Nusselt number was plotted against the radial location along the impingement plate. Nusselt number values were highest at the impingement point and decreased along the length of the impingement surface.

Ansu et al. used liquid crystal thermography to conduct experiments on effects of inlet conditions on heat transfer for single and multiple nozzle jet impingement [4]. Heat transfer co-

efficient were obtained for single and multi-nozzle jet impingement. Using hotwire anemometry length of the potential core was measured. Reynolds number was varied from 5000 to 15000 and distance between the nozzles was varied from 2D to 6D. Potential core length, Reynolds number, distance between the nozzles and parameters such as turbulent intensity were presented in relation to Nusselt number.

Guoneng et al. experimentally studied a row of jets impinging on a flat plate [5]. Reynolds number, jet height and ratio of jet velocity to laminar cross flow was investigated. The study showed that heat transfer can be increased with a series of circular jets if parameters such as separation distance can be optimized. Keeping all other parameters same, increase in Reynolds number, increases heat transfer. For small Reynolds number, as the jet height was decreased, Nusselt number was found to be decreasing. The authors also developed empirical equations for Nusselt number.

Using Tomographic Particle Image Velocimetry, Cafiero et al. carried out experiments on flow field generated by an impinging jet equipped with a fractal grid [6]. The Reynolds number was kept constant at 15,000. Due to fractal grid, non-uniform shear layer for jet was observed. Authors discussed the presence of azimuthally coherent structures generated due to Kelvin–Helmholtz instability of the jet shear layer.

Zhou et al. experimentally examined a single round air jet impinging on steel plate held at high temperature [7]. Heat transfer characteristics of jet impingement were obtained. Reynolds number was kept constant at 27,000 while the steel plate temperature was varied from 1073 K to 373 K. The distance between the nozzle was kept at 4D. At the initial stages of cooling the Nusselt number curve was observed to be bell shaped. As the time progressed, Nusselt number was seen to be decreasing with secondary peaks shown outside of the stagnation zone. The

average Nusselt number was observed to be in accordance with the Hofmann and Martin correlation.

Effect of the impinging fluid temperature, surface temperature and velocity of jet on the heat transfer characteristics was investigated by Wang et al [8]. It was observed that temperature of fluid and surface as well as velocity of the jet affected maximum heat flux. Empirical equation was established to predict heat flux values.

Ramezanpour et al. conducted CFD study on flat and inclined plate submerged jet impingement to calculate heat transfer rate [9]. The jet nozzle shape was rectangular. The inclined plate was held at 40 to 90 degrees, the Reynolds number was varied from 4000 to 16000 and nozzle height was kept at 4 to 10 times the hydraulic diameter. Heat flux of 100 w/m^2 was prescribed for the impingement surface. It was seen that the heat transfer rate was maximum at the stagnation point and decreased radially from stagnation point. A comparison was made with experimental results which showed less than 10% deviation.

De Bonis and Ruocco conducted review of existing procedures for analysis of heat transfer in case of jet impingement on food product [10]. Temperature and velocity plots were discussed. It was shown that combination of moisture and temperature gradients can be used to determine a strong process non-uniformity.

Dobbertean and Rahman analyzed steady state heating of patterned impingement surface by free liquid jet [11]. As the top surface of plate was cooled by impinging jet, a constant heat flux was applied to the bottom of the plate. Depth of indentations on the surface was varied along with Reynolds number. Heat transfer coefficient and Nusselt number were obtained. It was seen that Nusselt number increases with increase in Reynolds number. For rectangular pattern, heat

transfer coefficient was inversely proportional to the groove depth while for triangular patterns, heat transfer coefficient was directly proportional to groove depth.

Modak et al. theoretically studied two-dimensional jet impinging on a solid surface [12]. The solution was obtained using energy integral method. Along with theoretical approach, experiments were conducted to obtain the heat transfer characteristics of a two-dimensional jet impinging on hot surface. Height between nozzle and plate was varied from 1D to 10D and Reynolds number was varied between 7000 and 17000. Air was used as working fluid impinging on stainless steel foil. Infrared thermal imaging camera was used to observe heat transfer characteristics. A comparison between theoretical and experimental results showed close correlation. Nusselt number was shown to be dependent on nozzle to impingement surface distance, Reynolds number, radial location away from stagnation zone and Prandtl number.

Marcroft et al. used laser Doppler anemometer to measure the axial velocity of three and four jet arrays impinging on flat surface [13]. The study of velocity profiles showed jets exhibiting characteristics of a turbulent jet in its potential core region. Reverse flow was observed between neighboring jets. Velocity of reverse flow was measured to be 50 percent of the jet velocity. It also showed that depending on nozzle spacing and velocity of the jets, the product under multiple jet arrays might experience non-uniform heating.

Banooni et al. studied bread temperature, moisture content in the bread, color change and bread volume change during baking process [14]. Authors also explored effects of baking parameters on the attributes mentioned above. Hot air was used as working fluid. Baking time, velocity of jet and temperature of air was varied. Results showed temperature of impinging jet has much greater influence on baking than the velocity of jet. To optimize the quality of baking,

temperature was optimized while jet velocity was used to optimize the baking time. An algorithm was used to optimize baking parameters.

Effect of grid geometry on heat transfer rate during hot air jet impingement was studied by Cafiero et al. [15]. Geometry of initial pattern, grid thickness ratio and effect of grid interactions were taken into account. For smaller nozzle to impingement surface distance, larger thickness ratio was found to be beneficial. To obtain even distribution of heat transfer rate square as well as circular grid patterns were analyzed.

Alamir et al. proposed a model for French bread baking [16]. Experimental data was used to identify model parameters. Estimated potential energy savings of up to 16% were identified when using hot air impingement for bread baking.

For elliptical and rectangular jet impingement arrays, Caliskan et al. experimentally and numerically investigated the effect of geometry of a jet on heat transfer characteristics [17]. Using thermal infrared camera values of heat transfer coefficient were calculated. Laser-Doppler Anemometry was used for velocity measurements. Reynolds number, nozzle to surface distance and aspect ratio of the nozzle was varied. It was found that elliptical jets produced a larger Nusselt number compared to circular jets. Consequently, elliptical geometry was found to be more effective than circular geometry for heat transfer. Nusselt numbers for elliptic jets and rectangular jet were studied to understand correlation between the two geometries. Turbulent kinetic energy was calculated.

Terzis studied multiple jet impingement to understand correlation between flow structures and heat transfer [18]. Using high resolution instruments experiments were conducted for two narrow channels with a maximum crossflow and spacing over diameter ratio of 2 to 3.

Heat transfer coefficient was seen to be maximum at the stagnation point followed by secondary peaks.

Sarkar et al. reviewed turbulent characteristics of impinging hot air jets on food products [19]. Experimental approaches for single and multiple jet impingement were discussed. Methods used to measure heat transfer coefficient were presented. Impingement flow studies using laser doppler anemometry were reviewed. Also discussed briefly was the numerical modeling of impingement systems.

Variation in temperature, Nusselt number and heat transfer coefficient during multi-jet impingement was experimentally investigated by Chandramohan et al. [20]. The cooling application was considered. A constant heat flux was applied to the foil which in turn heated the flat plate that was directly in contact with the foil. Distance from nozzle to impingement surface was varied from 2D through 6D along with variation in nozzle diameter and Reynolds number. Smaller H/D ratio and larger Reynolds numbers resulted in higher heat transfer coefficients. Swirling was introduced in the jets and it was compared to jets without swirl. Swirling increased heat transfer for jets of diameter and 10 mm and 12 mm but for jet diameter of 8 mm it produced the opposite effect on heat transfer. H/D ratio and Reynolds number were found to have majority of the effect when it came to heat transfer between jets and impingement surface. Numerical simulations were verified by comparing it with known experimental results.

Garimella and Schroeder performed experiments on heat transfer of confined jets [21]. Jets of air at room temperature were impinged on heated surface. The orifice plate from which jets originated was mounted parallel to the impingement surface. The local surface temperature was measured in fine increments over the entire heat source. Reynold number and spacing between the jets was varied. In case of multiple jets, as the separation distance between nozzle

and impingement surface decreased, increase in heat transfer coefficient was noted. The effect was more pronounced at higher nozzle velocities With multiple jet configuration, the heat transfer to the center jet was higher than that of a single jet. The heat transfer coefficients in stagnation zone for a 4-nozzle arrangement were comparable to those of single nozzle jet. Correlations were proposed that would predict performance of single and multi-nozzle arrangements. It was found that nozzle spacing had an effect on local heat transfer coefficient. Equations governing relationship of average heat transfer coefficient to jet velocity, jet spacing, and Prandtl number were proposed.

Numerical simulations on multiple impinging jets were carried out by Penumadu and Rao [22]. To validate the model, the results were compared with known experimental results. The major contributing factors to pressure loss were found to be nozzle entrance contraction and viscous losses in the system. Simulations were also carried out to assess effect of manufacturing process tolerances on pressure loss.

Kannan and Sundararaj examined geometrical effects on the heat transfer of axisymmetric jet [23]. Flat and grooved plates were considered. Nozzle diameter was fixed at 2cm and nozzle to plate spacing of 4 cm and 8 cm was used. Jet was impinged with Reynolds number of 23000. Results showed secondary peaks in heat transfer as observed by other researchers. Grooves were found to have a negative effect on jet impingement heat transfer.

Numerical simulation of multiple jet impingement in oven was carried out by Kocer and Karwe [24]. The oven was assumed to be closed cavity with no interaction to the outside environment. Local heat transfer coefficient values were obtained on product surface. When compared with known experimental results, the simulation showed good agreement. Air temperature and velocity was varied. It was found that jet velocity had a higher impact on heat

transfer coefficient as compared to air jet temperature. Highest local heat transfer coefficient valves were found to be ~60 W/m^2K.

Review of the existing literature shows a majority of work related to single or multiple turbulent air jet impingement is experimental. Research related to systematically optimizing the controlling parameters of jet impingement using software analysis tools and then applying the lessons learned to a practical case study has not been thoroughly performed. The following research studies this un-explored area in great detail. The author has spent a great deal of effort ensuring the varying parameters are deeply rooted in real world applications.

In the next chapter jet impingement due to single nozzle is studied in detail. To establish validity of simulation, the simulation is compared with the known experimental results. A number of important parameters are studied to determine their interdependencies. This chapter forms the basis of more complex work that has been analyzed in further chapters.

CHAPTER 3: SIMULATION OF SINGLE NOZZLE JET IMPINGEMENT

In this chapter, convective heat transfer coefficient and its interdependency with various key parameters is analyzed for single nozzle turbulent jet impingement.

3.1 Modelling and Simulation

Configuration of un-bound jet configuration is shown in Figure 3.1. The applicable differential equations for the conservation of mass and momentum in the Cartesian coordinate system are [28],

$$\frac{\partial u}{\partial x}+\frac{\partial v}{\partial y}+\frac{\partial w}{\partial z}=0 \tag{1}$$

$$u\frac{\partial u}{\partial x}+v\frac{\partial u}{\partial y}+w\frac{\partial u}{\partial z} = -\frac{1}{\rho}\frac{\partial p}{\partial x}+\frac{\partial}{\partial x}\left[(v+v_t)\frac{\partial u}{\partial x}\right]+\frac{\partial}{\partial y}\left[(v+v_t)\frac{\partial u}{\partial y}\right]+\frac{\partial}{\partial z}\left[(v+v_t)\frac{\partial u}{\partial z}\right] \tag{2}$$

$$u\frac{\partial v}{\partial x}+v\frac{\partial v}{\partial y}+w\frac{\partial v}{\partial z} = -\frac{1}{\rho}\frac{\partial p}{\partial y}+\frac{\partial}{\partial x}\left[(v+v_t)\frac{\partial v}{\partial x}\right]+\frac{\partial}{\partial y}\left[(v+v_t)\frac{\partial v}{\partial y}\right]+\frac{\partial}{\partial z}\left[(v+v_t)\frac{\partial v}{\partial z}\right] \tag{3}$$

$$u\frac{\partial w}{\partial x}+v\frac{\partial w}{\partial y}+w\frac{\partial w}{\partial z} = -\frac{1}{\rho}\frac{\partial p}{\partial z}+\frac{\partial}{\partial x}\left[(v+v_t)\frac{\partial w}{\partial x}\right]+\frac{\partial}{\partial y}\left[(v+v_t)\frac{\partial w}{\partial y}\right]+\frac{\partial}{\partial z}\left[(v+v_t)\frac{\partial w}{\partial z}\right] \tag{4}$$

To simulate turbulence, the k-ε model was used. Equations governing the conservation of turbulence kinetic energy and its rate of dissipation are shown below,

$$u\frac{\partial k}{\partial x}+v\frac{\partial k}{\partial y}+w\frac{\partial k}{\partial z} \tag{5}$$
$$=\frac{\partial}{\partial x}\left[\left(v+\frac{v_t}{\sigma_k}\right)\frac{\partial k}{\partial x}\right]+\frac{\partial}{\partial y}\left[\left(v+\frac{v_t}{\sigma_k}\right)\frac{\partial k}{\partial y}\right]+\frac{\partial}{\partial z}\left[\left(v+\frac{v_t}{\sigma_k}\right)\frac{\partial k}{\partial z}\right]$$
$$+v_t\left[\left(\frac{\partial u}{\partial y}\right)^2+\left(\frac{\partial u}{\partial z}\right)^2+\left(\frac{\partial v}{\partial x}\right)^2+\left(\frac{\partial v}{\partial z}\right)^2+\left(\frac{\partial w}{\partial x}\right)^2+\left(\frac{\partial w}{\partial y}\right)^2\right]-\varepsilon$$

$$u\frac{\partial \varepsilon}{\partial x}+v\frac{\partial \varepsilon}{\partial y}+w\frac{\partial \varepsilon}{\partial z} \tag{6}$$
$$=\frac{\partial}{\partial x}\left[\left(v+\frac{v_t}{\sigma_\varepsilon}\right)\frac{\partial \varepsilon}{\partial x}\right]+\frac{\partial}{\partial y}\left[\left(v+\frac{v_t}{\sigma_\varepsilon}\right)\frac{\partial \varepsilon}{\partial y}\right]+\frac{\partial}{\partial z}\left[\left(v+\frac{v_t}{\sigma_\varepsilon}\right)\frac{\partial \varepsilon}{\partial z}\right]$$
$$+C_1\frac{\varepsilon}{k}v_t\left[\left(\frac{\partial u}{\partial y}\right)^2+\left(\frac{\partial u}{\partial z}\right)^2+\left(\frac{\partial v}{\partial x}\right)^2+\left(\frac{\partial v}{\partial z}\right)^2+\left(\frac{\partial w}{\partial x}\right)^2+\left(\frac{\partial w}{\partial y}\right)^2\right]$$
$$-C_2\frac{\varepsilon^2}{k}$$

$$v_t=C_\mu k^2/\varepsilon \tag{7}$$

The empirical constants appearing in equations (5)-(7) are given by the following values, $C\mu$=0.09, C_1=1.44, C_2=1.92, σ_k=1.0, σ_ε=1.3. The energy equation in the fluid region is,

$$u\frac{\partial T_f}{\partial x}+v\frac{\partial T_f}{\partial y}+w\frac{\partial T_f}{\partial z}=(\alpha+\frac{v_t}{Pr_t})\left[\frac{\partial^2 T_f}{\partial x^2}+\frac{\partial^2 T_f}{\partial y^2}+\frac{\partial^2 T_f}{\partial z^2}\right] \tag{8}$$

The equation for steady state heat conduction for solid region is [16],

$$\frac{\partial^2 T_s}{\partial x^2}+\frac{\partial^2 T_s}{\partial y^2}+\frac{\partial^2 T_s}{\partial z^2}=0 \tag{9}$$

To complete the physical model, equations (1) to (9) are subjected to the following boundary conditions:

$$\text{At } y = H+H_s,\ x= 0,\ z= 0 \tag{10}$$
$$V = V_{noz},\ u = 0,\ w = 0,\ T_{in} = 500^0F$$
$$\text{At } x=-L/2,\ -W/2<z<W/2,\ 0<y<H \tag{11}$$
$$\text{At } x=L/2,\ -W/2<z<W/2,\ 0<y<H$$
$$\text{At } z=-W/2,\ -L/2<x<L/2,\ 0<y<H$$

At $z=W/2$, $-L/2<x<L/2$, $0<y<H$

$$p=0$$

Initial conditions are:

At $y=0$, $-L/2<x<L/2$, $-W/2<z<W/2$ (12)

$$T_s=T_{amb}$$

For all configurations following parameters were kept constant, L=12.8 in, W=6.98 in, D=0.4375 in, $T_{in}=500^0$F. Finite volume method was used to solve the governing equations along with the boundary conditions. In each of the four-node quadrilateral element temperature, pressure and velocity fields were approximated leading to equations that established the continuum. During discretization process, the terms in the k-ε equations were linearized so numerical solution can be adequately converged. To solve the non-linear system of discretized equations, Newton-Raphson method was used. To arrive at a solution of temperature and velocity fields, an iterative procedure was used. When the field values did not change from one iteration to the next and the sum of residuals for each dependent variable became negligible, the solution was considered converged.

3.2 Results and Discussions

Figure 3.1 shows physical configuration of jet impingement model. Jet with Nozzle Velocity of V_{noz} and temperature of 500^0F travels through a distance H before hitting impingement surface of Length L and Width W. Sides of the 3D space are open to atmosphere making this an un-bound jet.

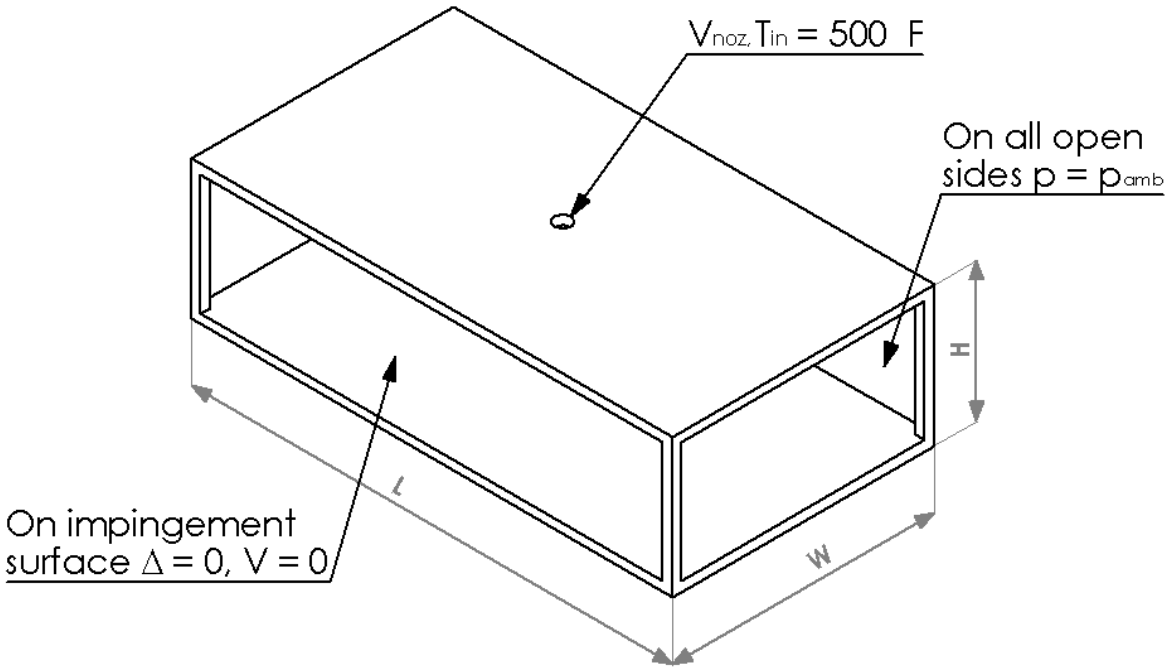

Figure 3.1: Physical configuration

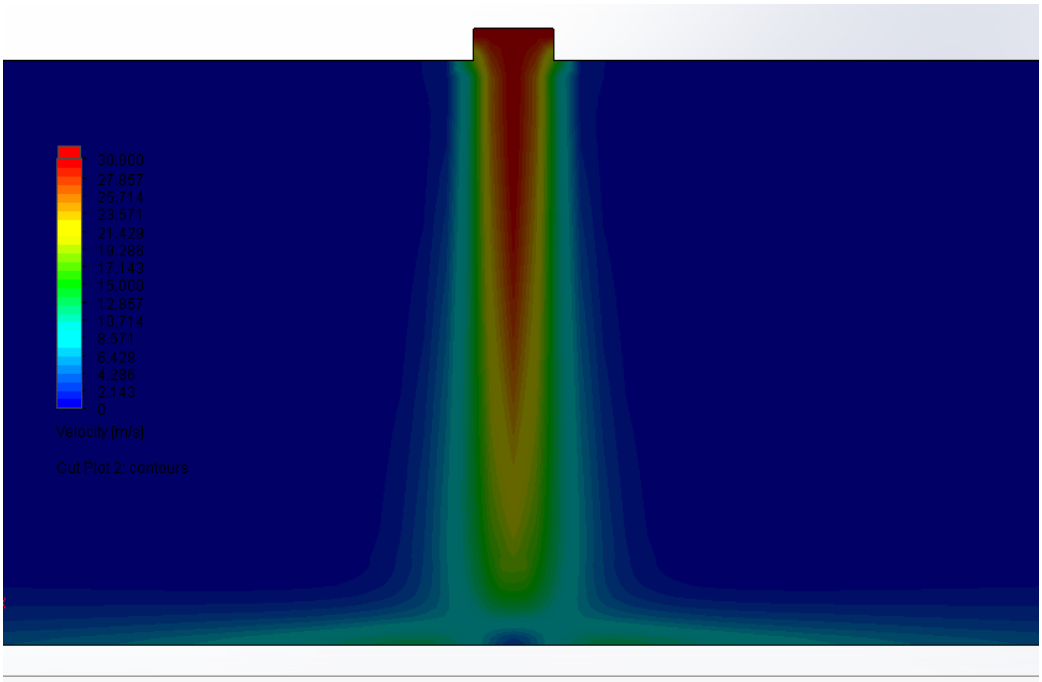

Figure 3.2: Velocity plot of single un-bound jet

Figure 3.2 shows CFD simulation of unbound jet with V_{noz} = 30 m/s and H/D ratio of 7, showing different regions as observed by Gardon and Akfirat [25] and later depicted by Sarkar and Singh [26]. Regions such as Potential Core, Mixing Region, Free jet Region, Stagnation Region and Radial Flow Region can be clearly seen in the simulation.

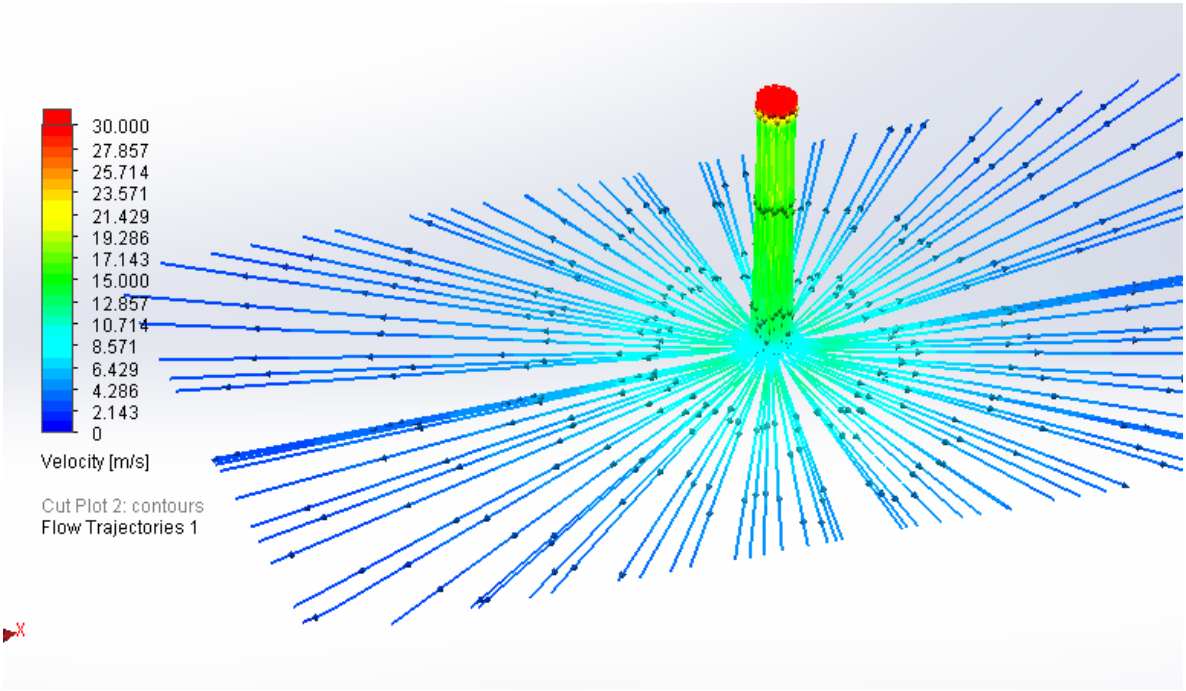

Figure 3.3: Flow trajectory of single un-bound jet

Figure 3.3 shows 3D representation of fluid trajectories of impinging jet. There is gradual decrease in fluid velocity due to mixing as the fluid flows towards impingement surface. After fluid hits the impingement surface where V = 0 m/s, there is a rapid increase in fluid velocity followed by gradual decrease along the impingement surface.

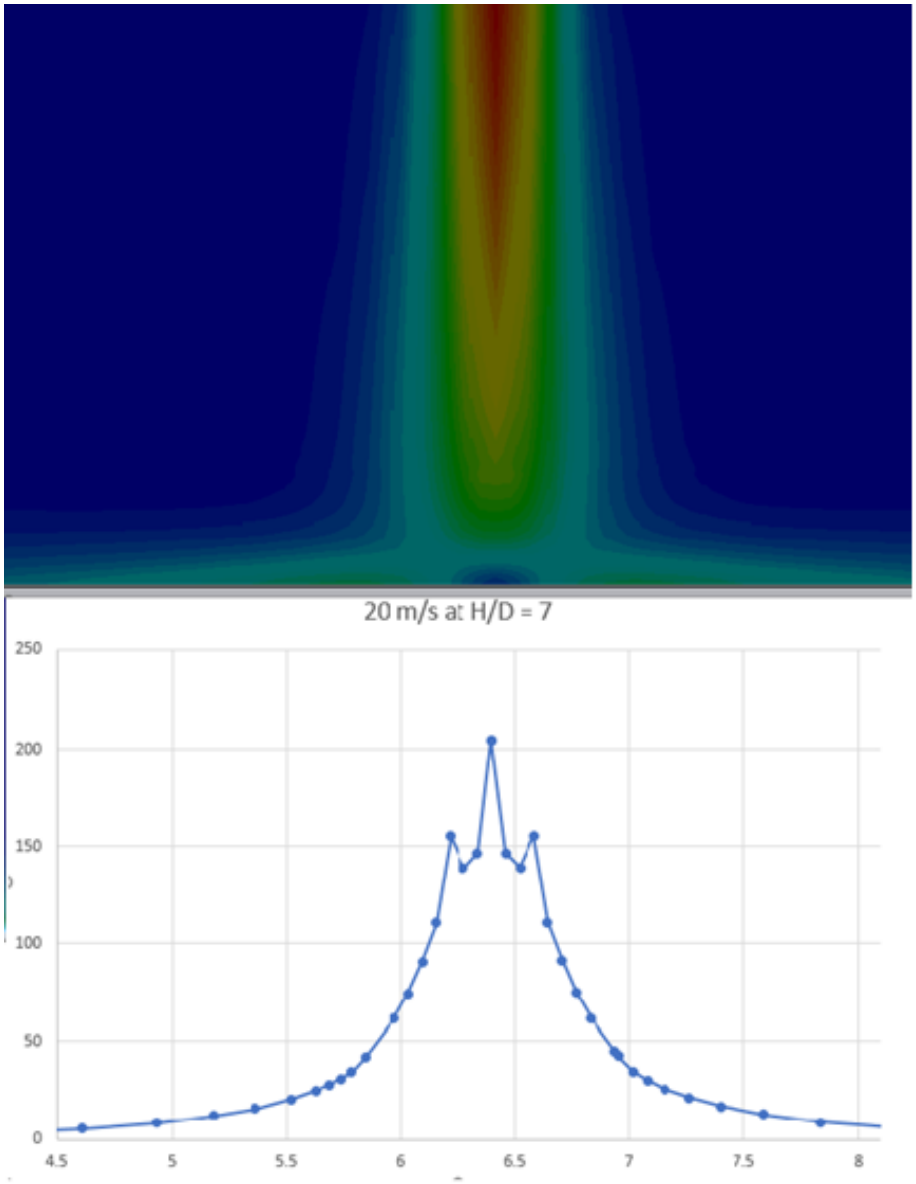

Figure 3.4: Heat transfer coefficient along impingement surface and its relation to velocity plot

Figure 3.4 shows details of heat transfer plot in relation to the velocity distribution. Highest peak in the heat transfer plot is at a stagnation point. The other two higher peaks occur outside boundaries of stagnation zone, where fluid accelerates before it starts slowing down along the impingement surface.

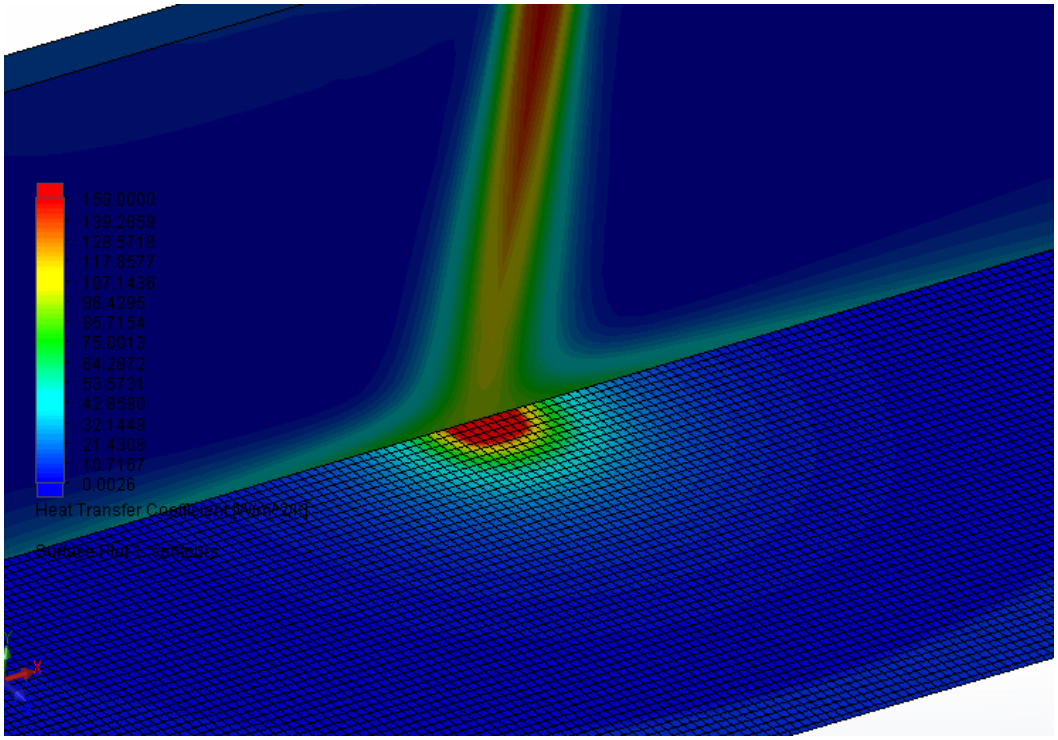

Figure 3.5: Heat transfer coefficient plot on the impingement surface and velocity profile on the front plane

Figure 3.5 shows heat transfer coefficient surface plot intersecting with velocity profile of a jet. Heat transfer coefficient is highest at the stagnation point. As the fluid velocity decreases along impingement surface, heat transfer coefficient decreases.

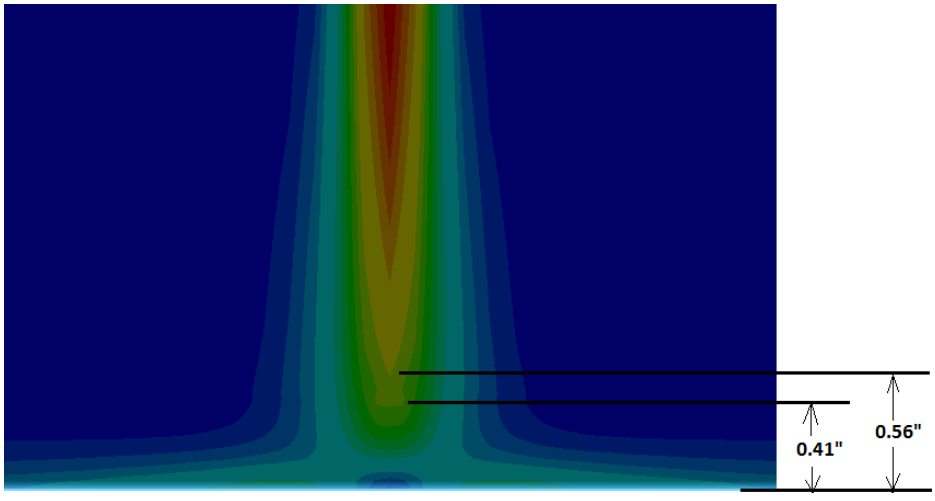

Figure 3.6: Velocity plot on the front plane and its relation to velocity degradation

Figure 3.6 shows velocity plot of impinging jet at V_{noz} = 20 m/s and H/D ratio of 7. Nozzle diameter is 0.4375". As the fluid approaches stagnation zone, there is a rapid degradation of velocity along the nozzle centerline. The degradation occurs at a distance equal to D – 1.5D from the impingement surface. This trend as shown in Figure 3.13 is common over a range of velocities and H/D ratios.

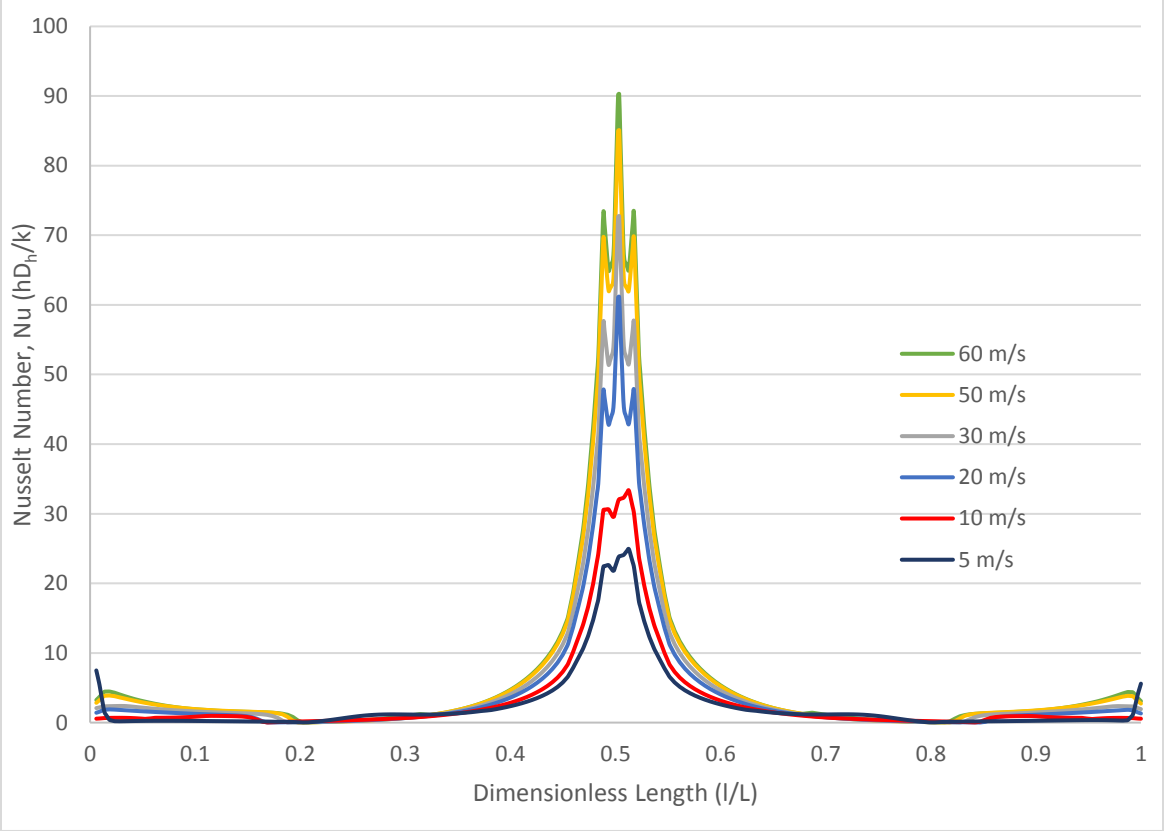

Figure 3.7: Nusselt number vs dimensionless length along impingement surface for different nozzle velocities (H/D =7)

Figure 3.7 shows Nusselt number values along the impingement surface for H/D ratio of 7. For a fixed H/D ratio of 7, Nusselt number increases with increase in nozzle velocity but percentage increase beyond 20 m/s is less than percentage increase from 10 m/s to 20 m/s. Nozzle velocities higher than 30 m/s may be detrimental to cooking process since lighter food particles may become airborne at higher nozzle velocities.

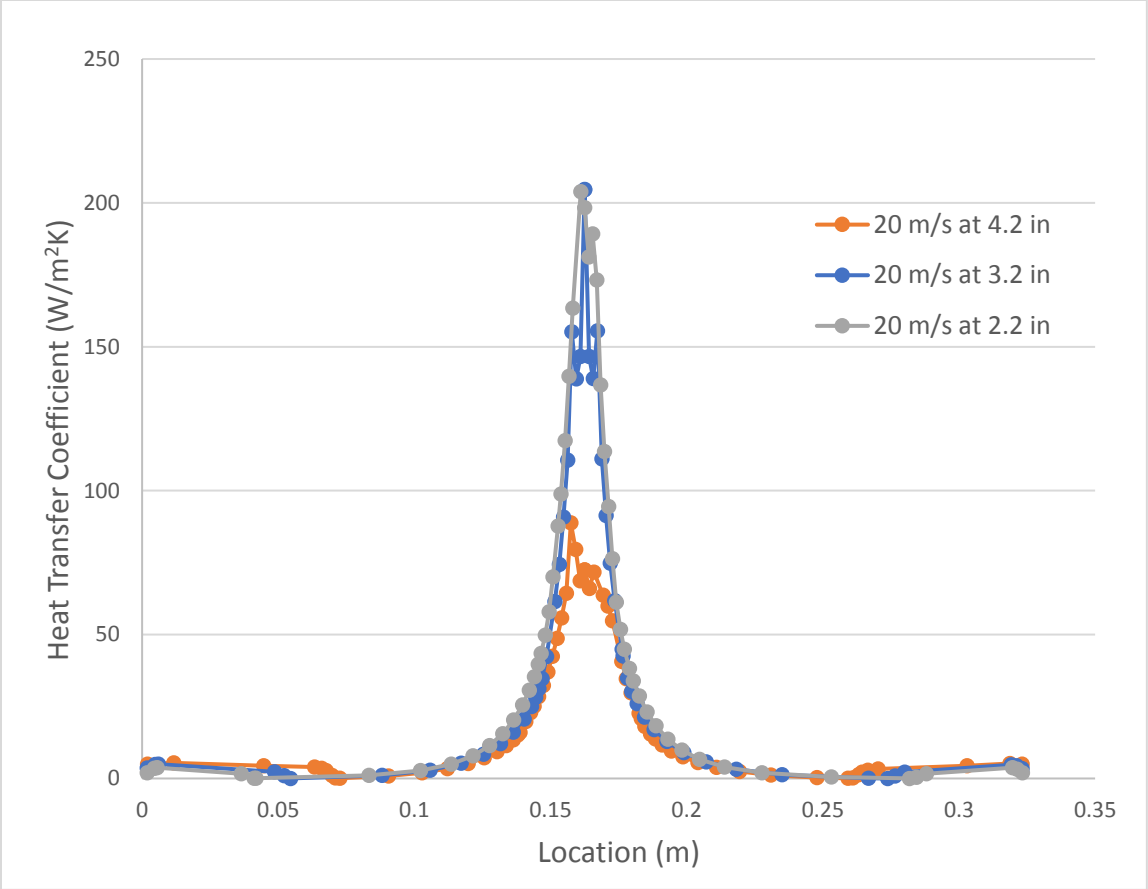

Figure 3.8: Heat transfer coefficient vs location on impingement surface for different H/D ratios

Figure 3.8 shows heat transfer coefficient along the impingement surface for different values of H/D ratio. Heat transfer coefficient is seen inversely proportional to the H/D ratio. As H/D ratio is increased above 8, there is a rapid decrease in heat transfer coefficient. Increase in heat transfer coefficient is not sufficient enough to warrant decrease in H/D ratios below 6. It is also practically difficult to decrease H/D ratio below 6 since sufficient distance is required between nozzle and impingement surface so food can be placed below the nozzle.

Figure 3.9 shows Turbulent Energy variation along the impingement surface for different H/D ratios and V_{noz} = 30 m/s. As H/D ratio is decreased, Turbulent Energy increases. Turbulent Energy dissipates at a lower rate for higher H/D ratio due to increased distance between nozzle and impingement surface.

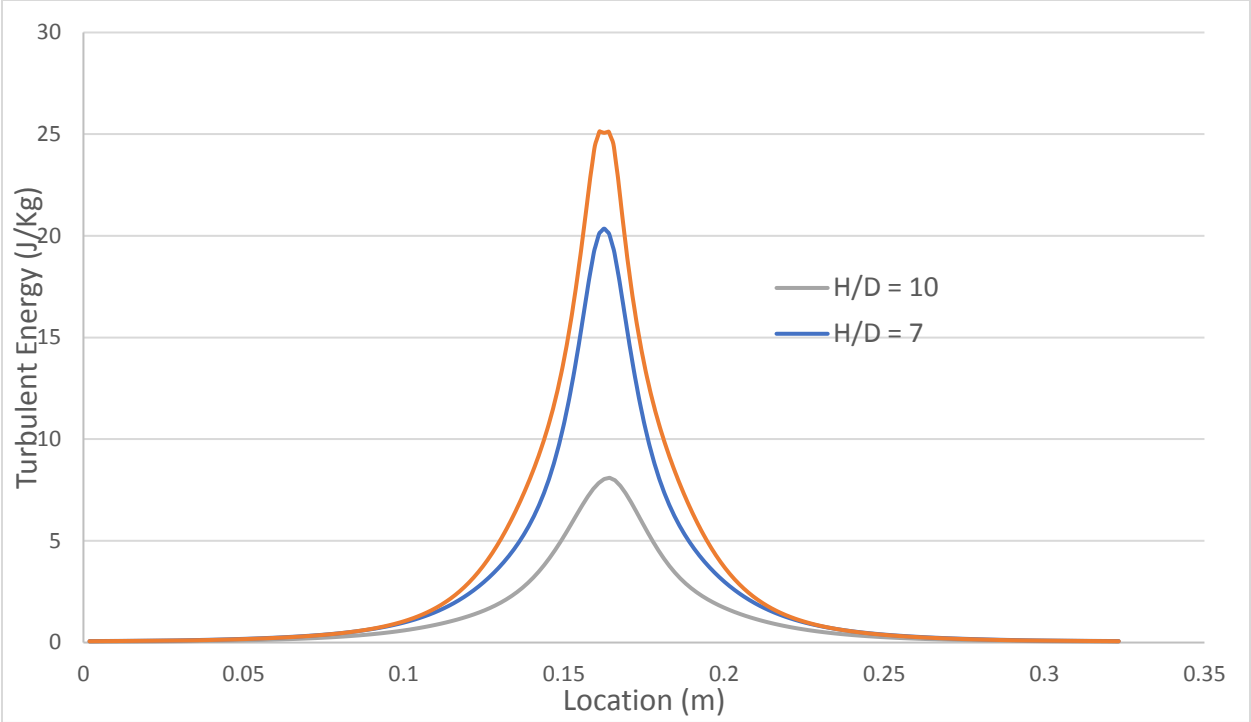

Figure 3.9: Turbulent energy along the impingement surface for V_{noz} = 30 m/s

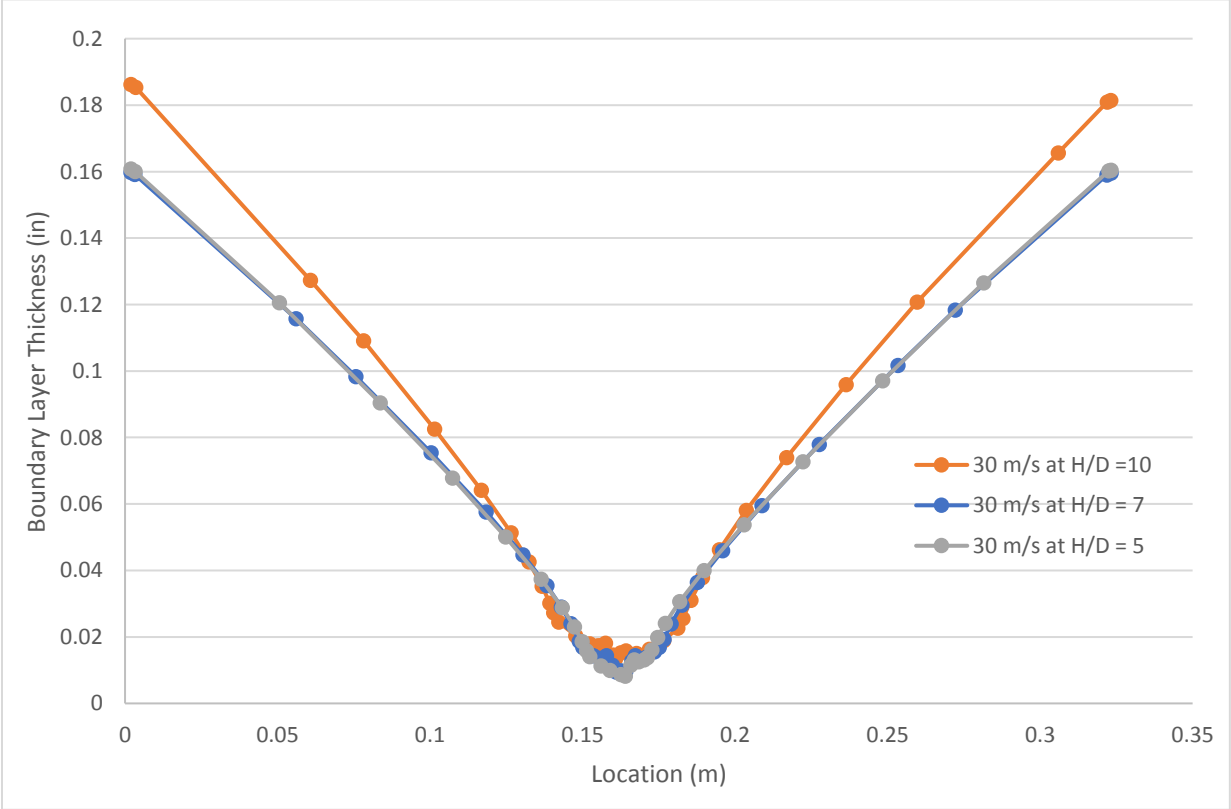

Figure 3.10: Boundary layer thickness along impingement surface vs location

Figure 3.10 shows boundary layer thickness along the impingement surface. The graph shows, boundary layer thickness decreases along with decrease in H/D ratio. For H/D ratios below 7, the decrease in boundary layer thickness is negligible. Lower values of boundary layer thickness are advisable since increase in boundary layer thickness impedes heat transfer process.

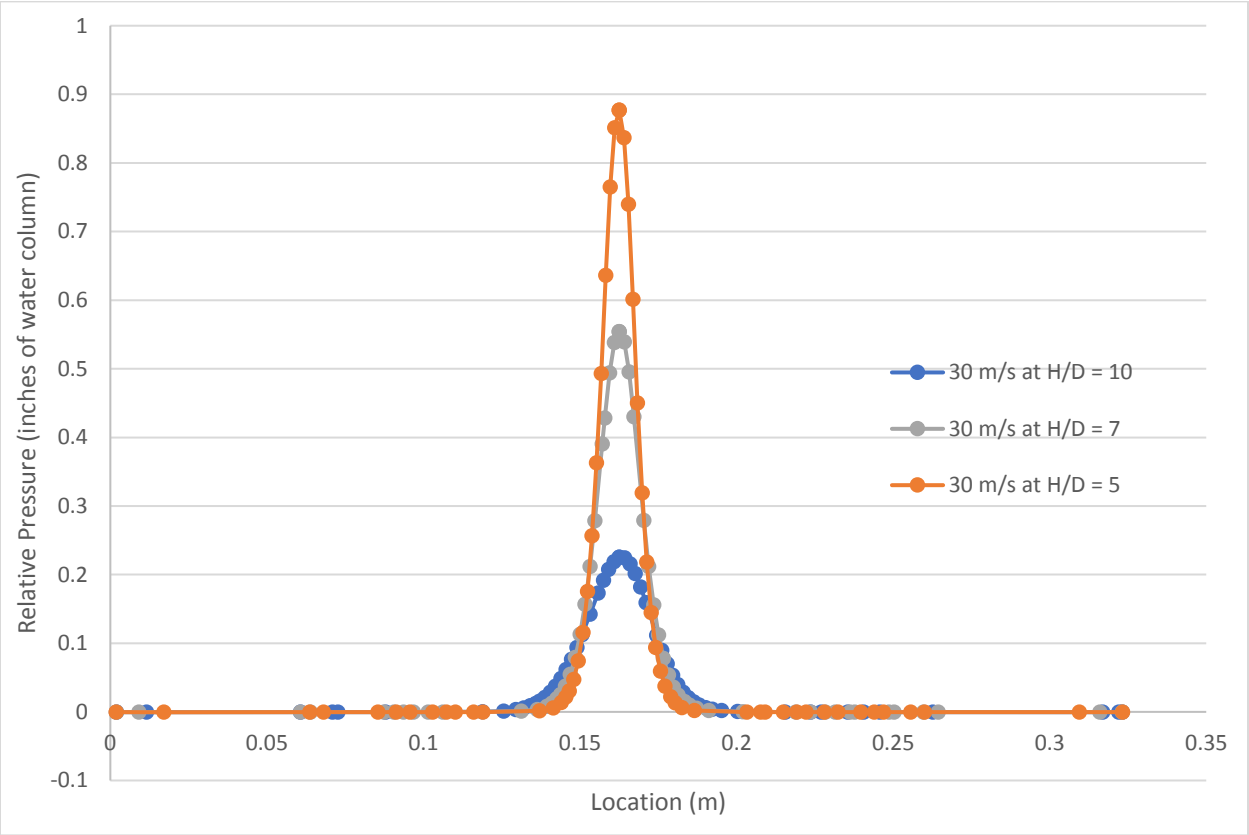

Figure 3.11: Relative pressure vs location along impingement surface

Figure 3.11 shows relation between relative pressure and its location along impingement surface. Pressure rises rapidly near stagnation zone reaching its peak value at stagnation point. In foodservice industry depending upon the product being cooked, high values of relative pressure could be counter-productive since they may affect integrity of food.

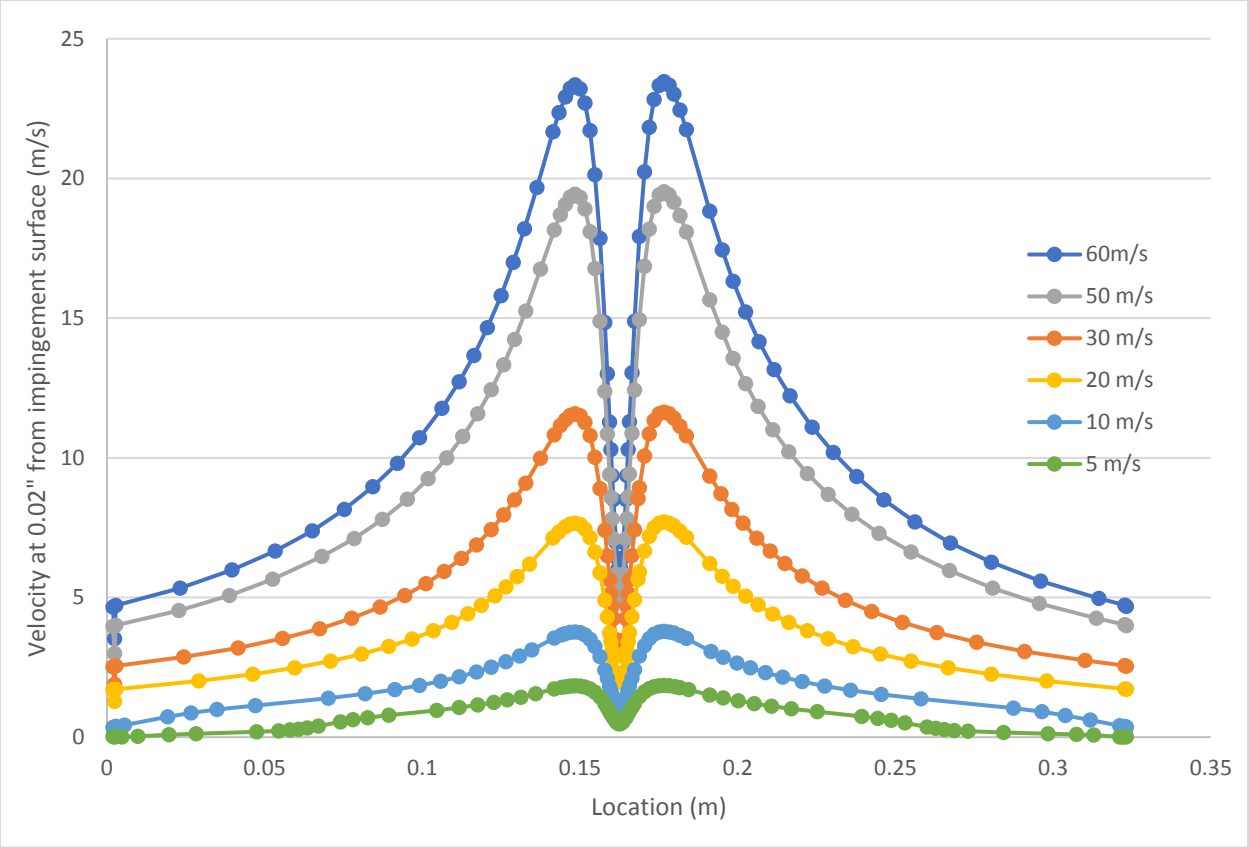

Figure 3.12: Fluid velocity at 0.020” away from the impingement surface

Figure 3.12 shows fluid velocity plot 0.020” away from the impingement surface along the front plane. After air impinges straight down at stagnation point where fluid velocity is zero, it accelerates rapidly up to a certain distance along the horizontal surface followed by a gradual decrease in velocity along the surface.

Figure 3.13 shows fluid velocity along the nozzle centerline. Fluid velocity was plotted for different velocities and different H/D ratios. The graph shows that, irrespective of fluid velocity and H/D ratio, velocity values show a rapid degradation at a distance approx. D to 1.5D from the impingement surface. This zone is called Stagnation Zone. Fluid velocity is zero at the center of stagnation zone.

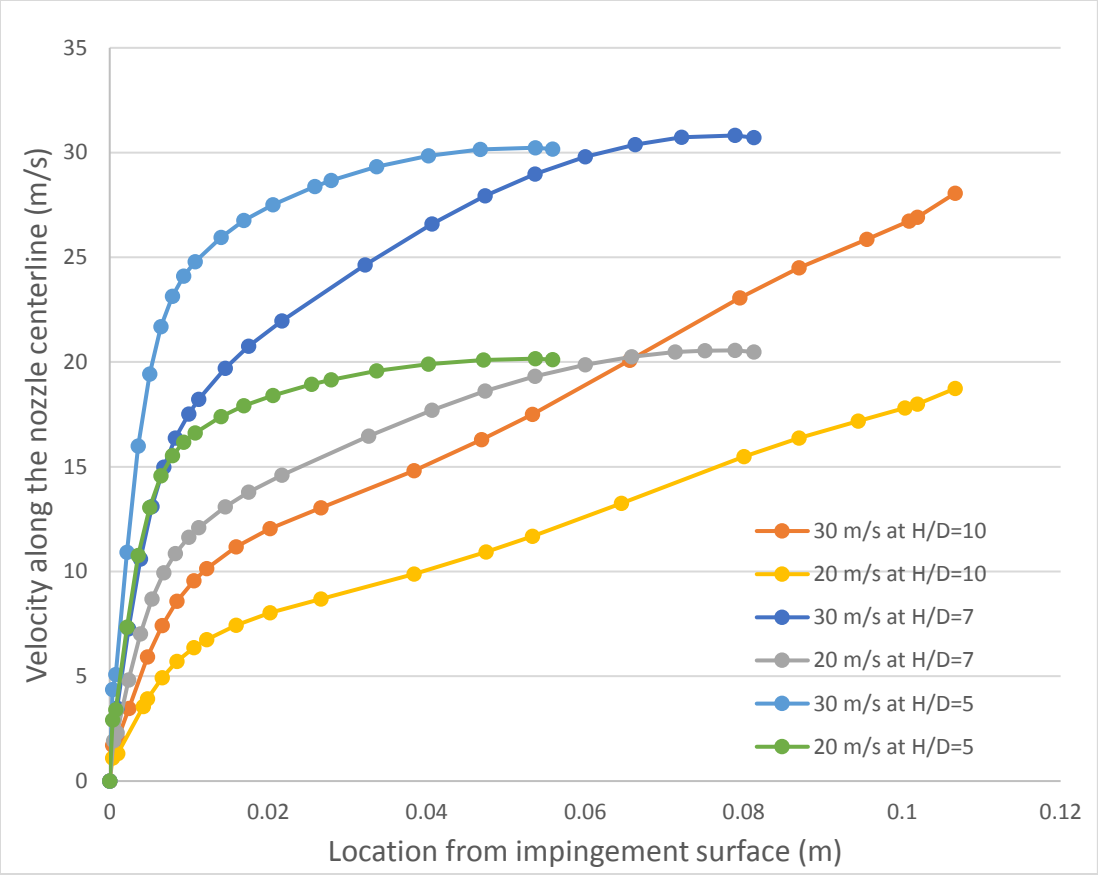

Figure 3.13: Fluid velocity along nozzle centerline

3.3 Conclusions

Analysis and optimization of different controlling parameters during single jet impingement shows clear interdependencies between parameters such as Nozzle Velocity and H/D ratio. Highest values of heat transfer coefficient occur at stagnation point. The next higher peak occurs outside the boundaries of stagnation zone where air accelerates before it starts slowing down along the impingement surface. The height of stagnation zone is found to be at a distance D to 1.5D from the impingement surface. This zone is characterized by rapid decrease in air velocity. Heat transfer coefficient values are highest for H/D ratios between 6 and 8. For a fixed nozzle velocity, boundary layer thickness decreases with decrease in H/D ratio.

The next chapter builds on single nozzle jet impingement to analyze multi-nozzle jet impingement and it is a step closer to analyzing a real-world scenario. When multiple nozzles are present, the interaction between neighboring nozzles becomes an important part of the analysis. The next chapter provides several key parameters which affect the heat transfer in multi-nozzle turbulent flow field.

CHAPTER 4: SIMULATION OF MULTI-NOZZLE JET IMPINGEMENT

In this chapter, convective heat transfer coefficient and its interdependency with various key parameters is analyzed for turbulent multi-jet impingement.

4.1 Modelling and Simulation

Physical configuration of un-bound jet configuration is shown in Figure 4.1. The applicable differential equations for the conservation of mass and momentum in the Cartesian coordinate system are equations 1 through 9 from chapter three,

To complete the physical model, equations are subjected to the following boundary conditions:

$$\text{At } y=H+Hs,\ x=0,\ z=0 \qquad (10)$$

$$v=V_{noz},\ u=0,\ w=0,\ Tin = 500^0F$$

$$\text{At } x=-L/2,\ -W/2<z<W/2,\ 0<y<H \qquad (11)$$

$$\text{At } x=L/2,\ -W/2<z<W/2,\ 0<y<H$$

$$\text{At } z=-W/2,\ -L/2<x<L/2,\ 0<y<H$$

$$\text{At } z=W/2,\ -L/2<x<L/2,\ 0<y<H$$

$$p=0$$

Initial conditions are:

$$\text{At } y=0,\ -L/2<x<L/2,\ -W/2<z<W/2 \qquad (12)$$

$$T_s=T_{amb}$$

For all configurations following parameters were kept constant, L=12.8in, W=5in, T_{in}=500 ^{0}F (260^{0}C). Finite volume method was used to solve the governing equations along with the boundary conditions. In each of the four-node quadrilateral element temperature, pressure and velocity fields were approximated leading to equations that established the continuum. During discretization process, the terms in the k-ε equations were linearized so numerical solution can be adequately converged. To solve the non-linear system of discretized equations, Newton-Raphson method was used. To arrive at a solution of temperature and velocity fields, an iterative procedure was used. When the field values did not change from one iteration to the next and the sum of residuals for each dependent variable became negligible, the solution was considered converged.

Table 4.1: Simulation structure for multi-nozzle jet impingement

Simulations	H (in)	S (in)	D (in)	H/D	S/D
sim1	3.2	3.2	0.4375	7	7
sim2	3.2	3.2	0.3125	10	10
sim3	3.2	4.2	0.4375	7	10
sim4	4.2	3.2	0.4375	10	7
sim5	4.2	3.2	0.3125	13	10
sim6	1.8	3.2	0.4375	4	7
sim7	3.2	3.2	0.625	5	5
sim8	3.2	1.8	0.4375	7	4
sim9	3.2	2.6	0.4375	7	6

Table 4.1 shows number of simulations that were carried out to study the effect of Nozzle Velocity, H/D ratio and S/D ratio on heat transfer coefficient, average impingement surface temperature and heat transfer rate. Standard drill sizes were used as nozzle diameters.

4.2 Results and Discussions

Figure 4.1 shows physical configuration of multi-jet impingement model. For all simulations 3 equally spaced nozzles are used. Jet with Nozzle Velocity of V_{noz} and temperature of 500 ^{0}F (260^{0}C) travels through a distance H before impinging on surface of Length L and Width W. Sides of the 3D space are open to atmosphere making this an un-bound jet.

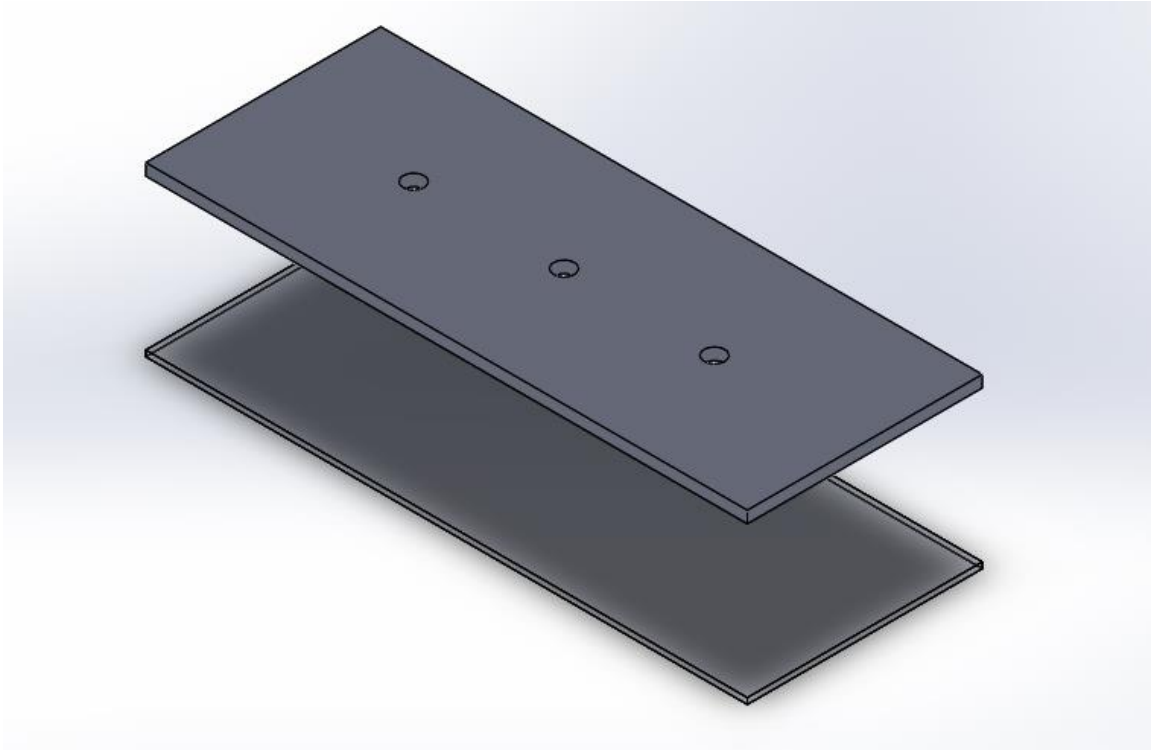

Figure 4.1: Physical configuration

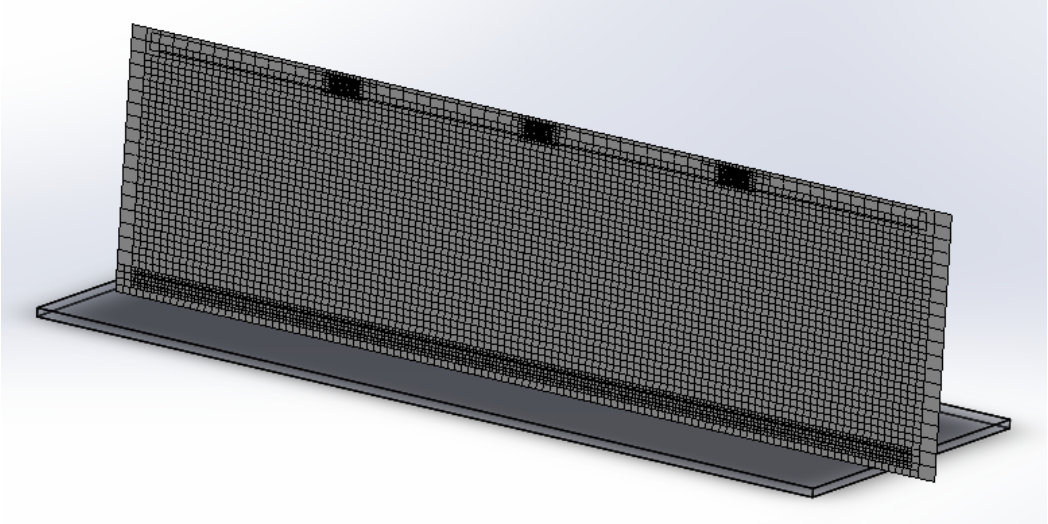

Figure 4.2: Mesh structure for 3 nozzle arrangement

Figure 4.2 shows mesh used for this simulation. A mesh independence study was carried out to arrive at the optimum mesh size. The total number of mesh elements are approximately 450,000.

To validate the model, the simulation was compared with the experimental results obtained by Caliskan et al. [17]. As shown in Figure 4.3, for Re=2000 and H/D = 2, with variance of less than 10%, the simulation showed good agreement with the experimental results.

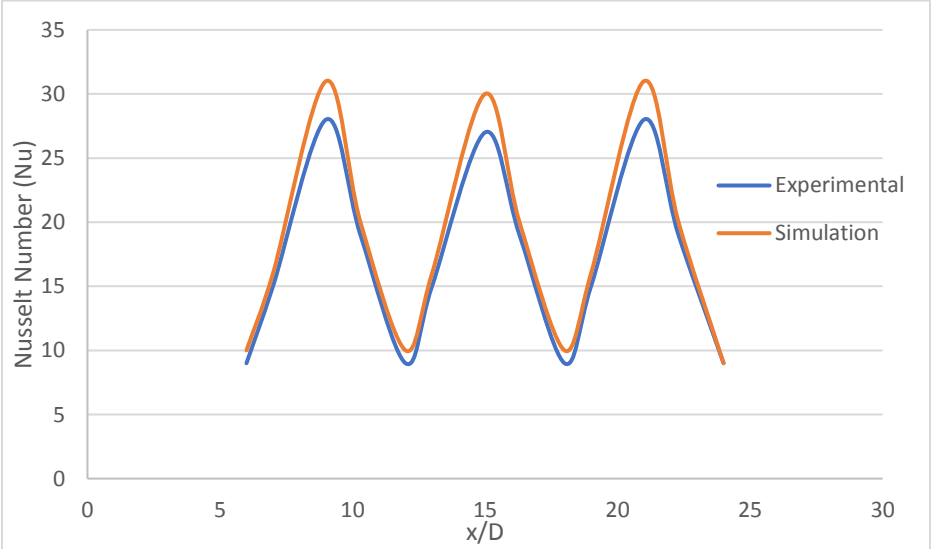

Figure 4.3: Model validation

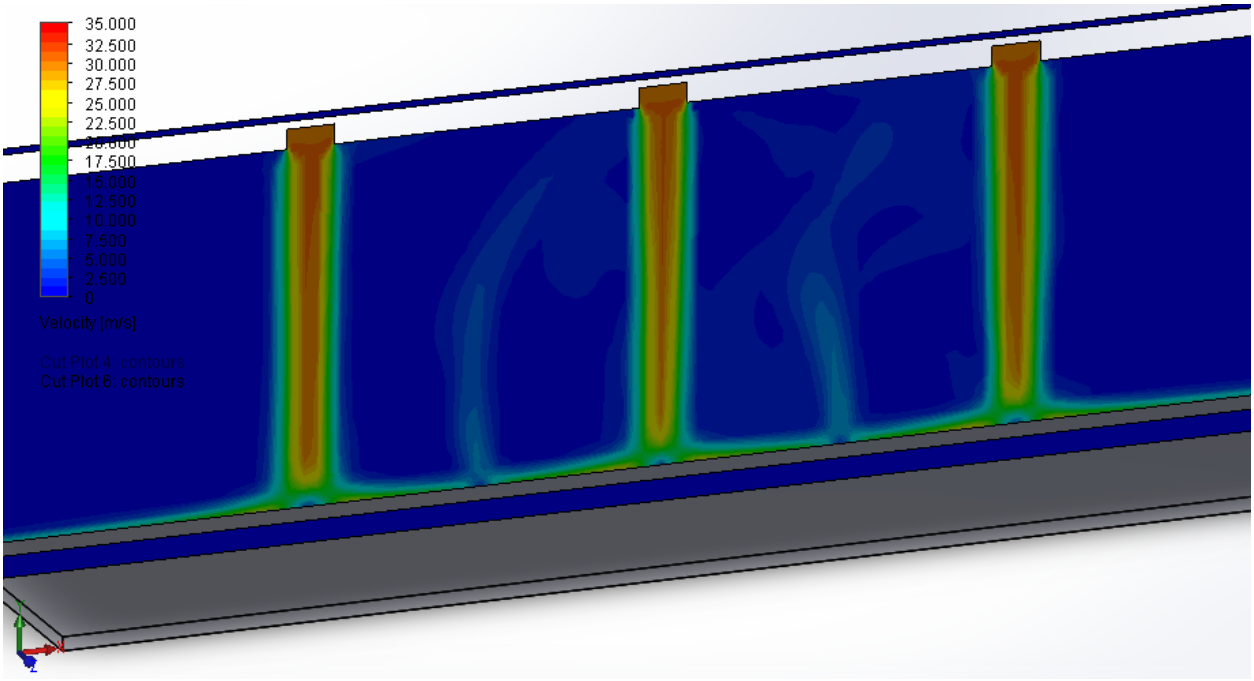

Figure 4.4: Velocity cut plot for 3 nozzle arrangement

Figure 4.4 shows CFD simulation of multi-jet impingement with V_{noz} = 30 m/s, H/D ratio of 7 and S/D ratio of 7, showing different regions as observed by Gardon and Akfirat [25] and later depicted by Sarkar and Singh [26]. Regions such as Potential Core, Mixing Region, Free jet Region, Stagnation Region and Radial Flow Region can be clearly seen in the simulation. A reverse flow region as noted by Marcroft et al. [27] is also seen in between two jets.

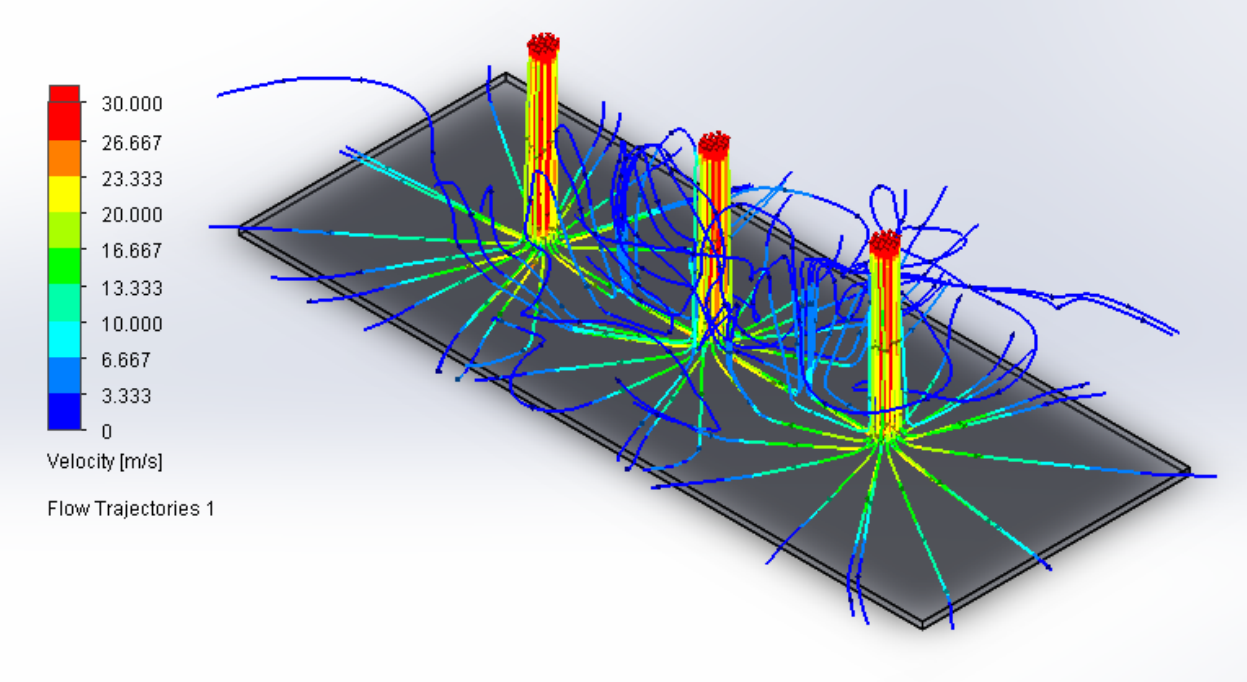

Figure 4.5: Flow trajectory for 3 nozzle arrangement

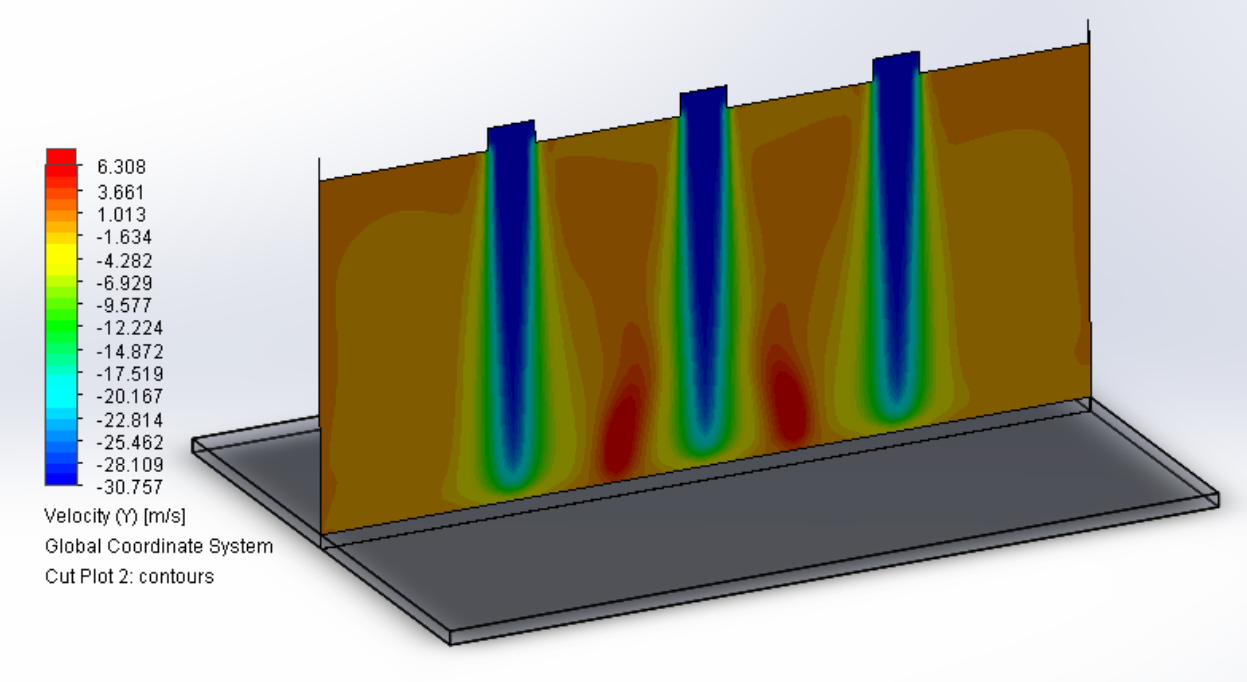

Figure 4.6: Velocity in Y (vertical) direction

Figure 4.5 shows 3D representation of fluid trajectories of impinging jets. There is a gradual decrease in fluid velocity due to mixing as the fluid flows towards impingement surface.

After fluid hits the impingement surface where V = 0 m/s, there is a rapid increase in fluid velocity followed by gradual decrease along the impingement surface. As seen in the trajectories, mixing of the adjacent jets occurs which leads to uneven heat transfer across the impingement surface. This can be controlled by varying S/D ratio which is studied later in this chapter.

Figure 4.6 shows cut plot of velocity in y-direction (vertical) for S/D ratio of 4. The plot helps visualize the reverse airflow which extends up to half the vertical distance between nozzle and impingement surface (H).

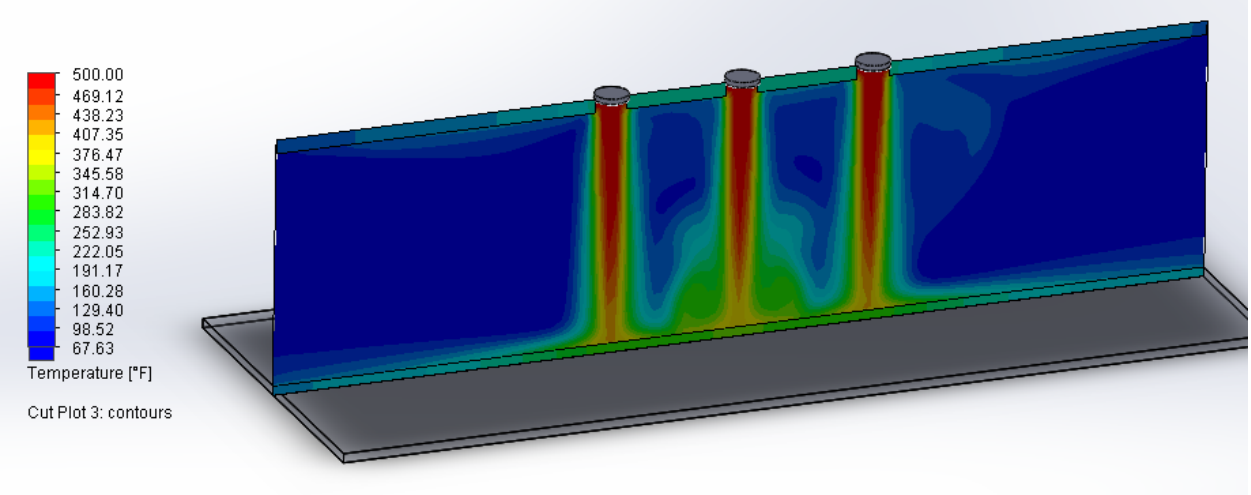

Figure 4.7: Temperature cut plot

Figure 4.7 shows air temperature distribution of 3 nozzle jet interaction. All jets are at 500 ^{0}F while the surrounding air is at ambient temperature. At V_{noz} of 30 m/s, H/D ratio of 7 and S/D ratio of 4, core of the jet retains its temperature as it proceeds towards impingement area. There is a rapid decrease in air temperature as the jet exchanges heat with impingement surface. Hot spots of air between interacting jets show that not all energy in the air has been exchanged with the impingement surface. This can be further improved by varying controlling parameters.

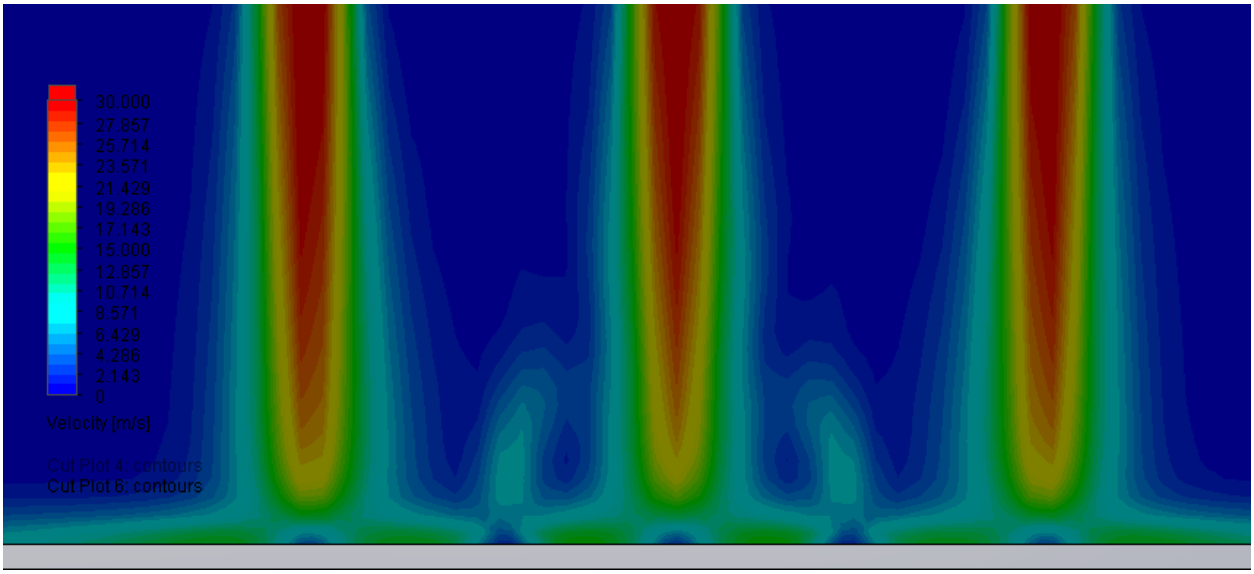

Figure 4.8: Jet core shift due to multi-jet interaction

Figure 4.8 shows effect of multi-jet interaction on the tip of the jet core region for S/D ratio of 4. Due to the air flow from the center jet the tips of the outer jets are seen to be shifting outwards. The effect is more pronounced at lower S/D ratios due to increased interaction with center jet. At low S/D ratios this can lead to severe non-uniform heat transfer.

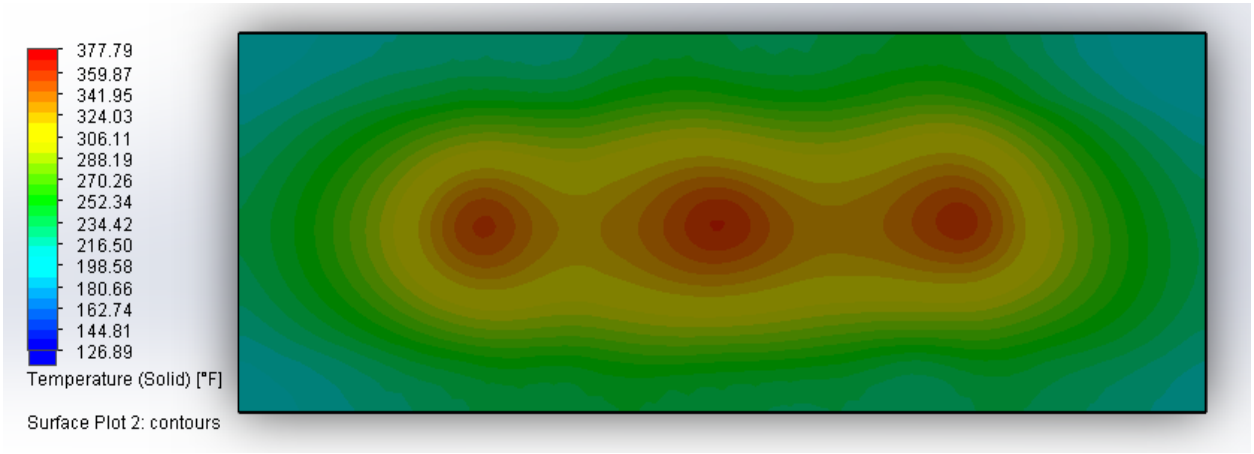

Figure 4.9: Surface temperature plot

Figure 4.9 shows surface temperature plot of impingement surface for V_{noz} = 30 m/s, H/D ratio of 7 and S/D ratio of 7. The heat transfer due to single impinging jet is highly localized but

when jets are placed in series the interaction between the jets helps bridge the area between the individual jets increasing total heat transfer to the impinging surface.

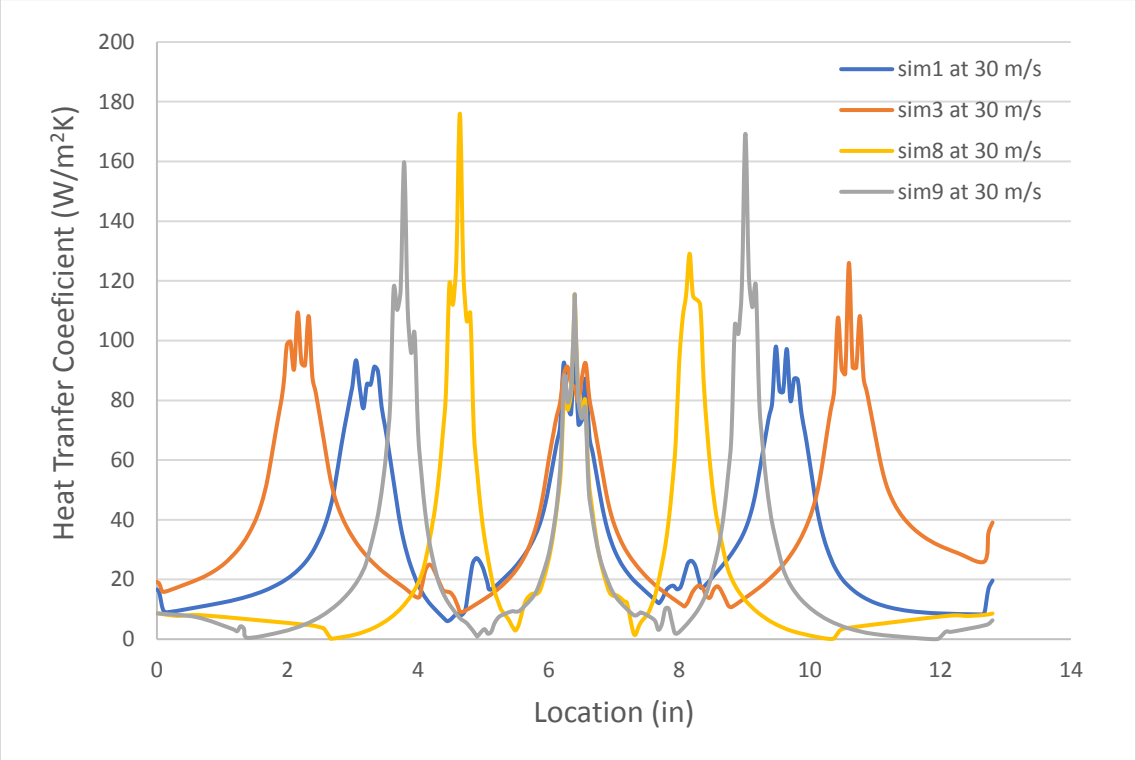

Figure 4.10: Heat transfer coefficient along the surface for different S/D ratios

Figure 4.10 shows heat transfer coefficient plot along the impingement surface for different S/D ratios. V_{noz} is kept constant at 30 m/s and H/D ratio for all data points is kept at 7. The graph shows optimum S/D value of 7 for uniform distribution of heat transfer coefficient for all three nozzles. As the S/D value is decreased to 6, higher values of local heat transfer coefficient can be achieved at the expense of uniformity of heat transfer for the three nozzles. Cooking food uniformly is essential so higher peaks for outer nozzles compared to center nozzle are not preferable. For S/D ratio of 4 and below, the nozzles are too close together which increases the reverse flow between nozzles creating uneven heat transfer peaks that drop rapidly creating less than required coverage over the impingement area. For S/D ratio of 10, the nozzles are spread too far apart. This creates higher heat transfer values for individual nozzles but does

not provide adequate coverage over the entire impingement surface bringing down the average heat transfer coefficient.

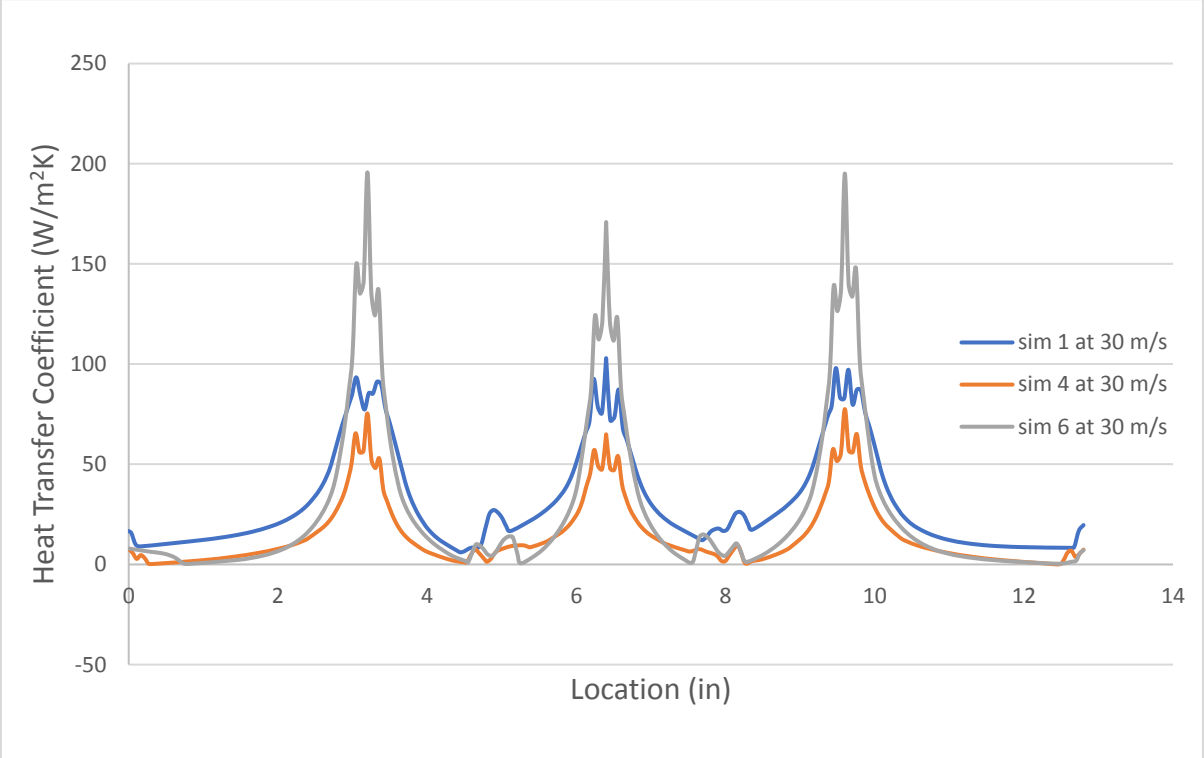

Figure 4.11: Heat transfer coefficient along the surface for different H/D ratios

Figure 4.11 shows heat transfer coefficient plot along the impingement surface for different H/D ratios. V_{noz} is kept constant at 30 m/s and S/D ratio for all data points is kept at 7. The graph shows local heat transfer values are inversely proportional to H/D ratio. As the distance between the nozzle and impingement surface is decreased, higher heat transfer coefficient peaks are achieved. The high peaks at H/D ratio of 4 deteriorate more rapidly along the impingement surface compared to the more uniform peaks for H/D ratio of 7. For H/D ratio of 10, the higher distance between nozzle and impingement surface creates lower values of heat transfer coefficient.

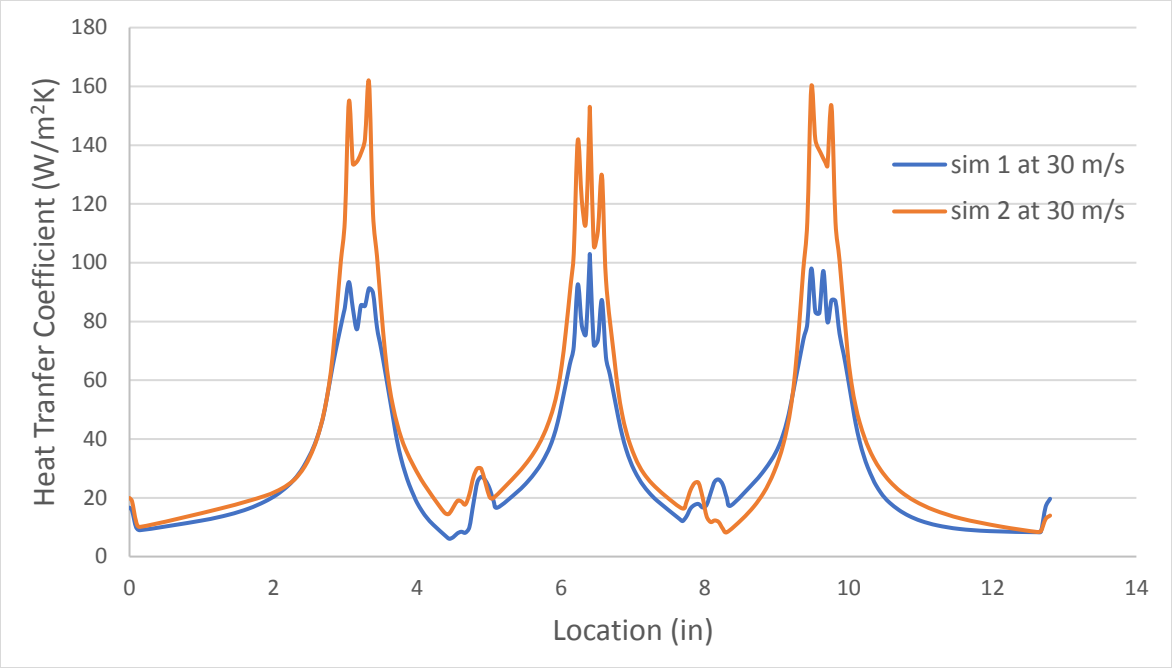

Figure 4.12: Heat transfer coefficient along the surface for different diameters

Figure 4.12 shows graph of heat transfer coefficient for different nozzle diameters for V_{noz} of 30 m/s. For a particular velocity, heat transfer coefficient values are directly proportional to nozzle diameter. This does have practical limitations. To maintain the same velocity with bigger diameter nozzle, a bigger fan is required to drive the air. This might be physically restrictive due to size or not preferable due to energy consumption and material cost.

Figure 4.13 shows average temperature of the impingement surface for different nozzle diameters at different nozzle velocities. The trend confirms the statement made above in regard to relation between heat transfer coefficient and nozzle diameter for a particular velocity. It also shows interesting trends about the decrease in average surface temperature above a limiting velocity. In case of D = 0.4375 inch, this limiting velocity is approximately 40 m/s whereas in case of D = 0.3125 inch, the limiting velocity is 30 m/s. Above this limiting velocity the interaction between neighboring jets is highly turbulent and unpredictable which results in high

amounts of ambient air being introduced in the control volume, reducing the overall average temperature of the impingement surface.

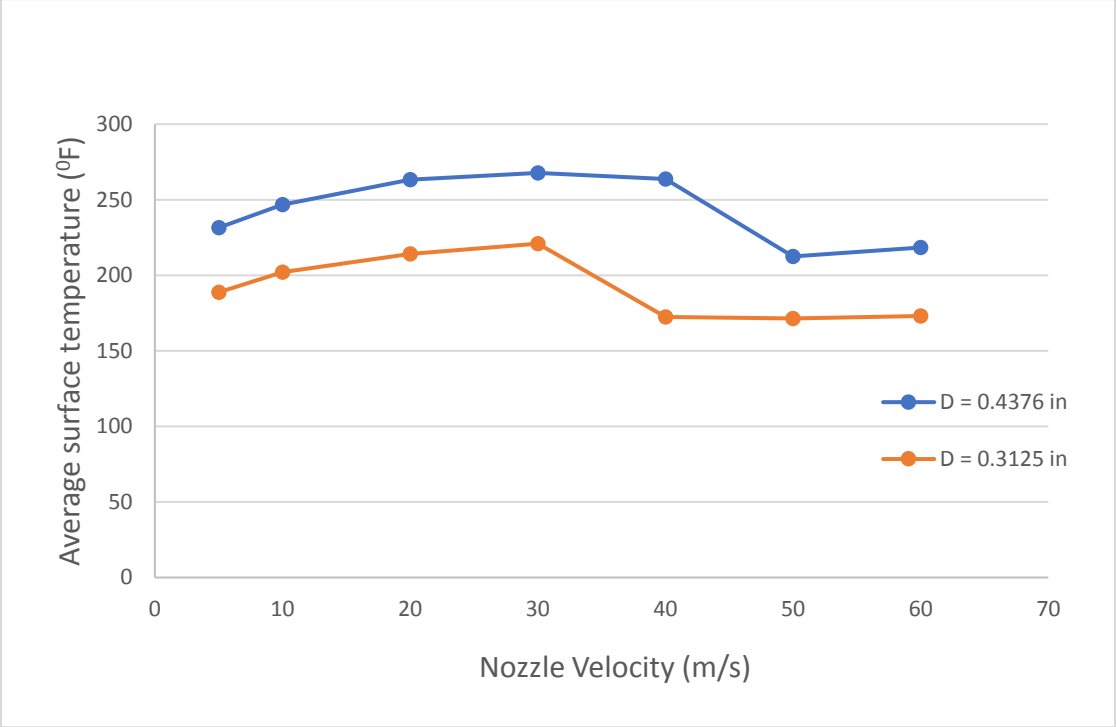

Figure 4.13: Average plate temperature at different velocities for different diameters

Figure 4.14 shows heat transfer rate on the impingement surface for different nozzle velocities for S/D and H/D ratio of 7. Heat transfer rate increases as the nozzle velocity increases until it reaches a limiting value. As nozzle velocity is increased further above 40 m/s, there is drop in heat transfer rate due to ingress of large amounts of cold ambient air in the control volume.

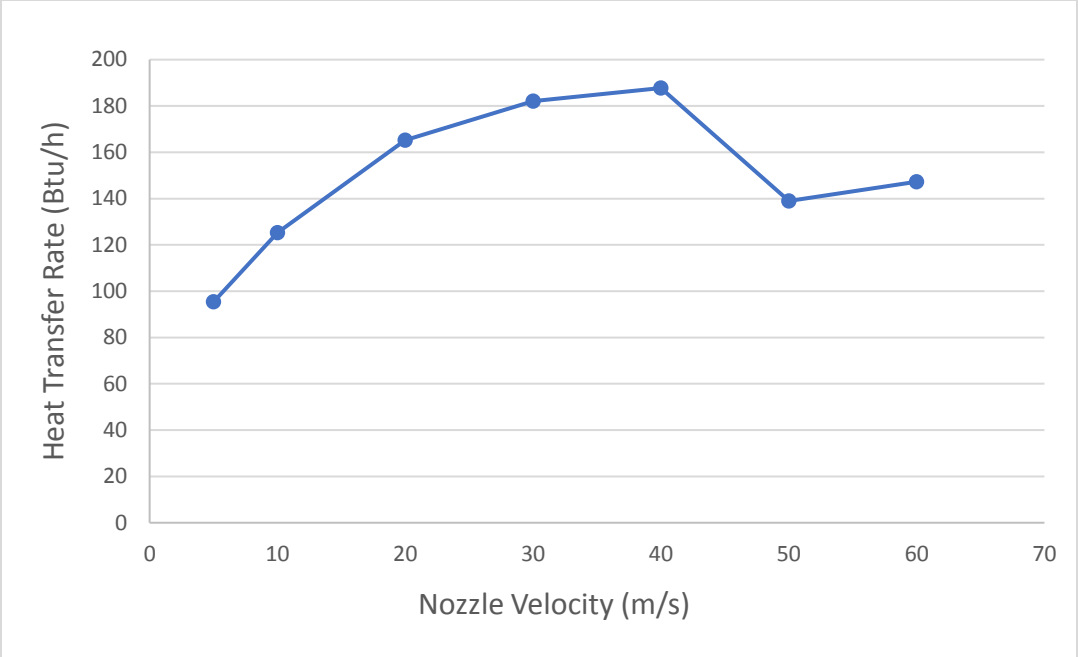

Figure 4.14: Heat transfer rate at different velocities

Figure 4.15 shows average impingement surface temperature for different H/D ratios. Smaller H/D ratios yield higher average surface temperature. Within the same H/D ratio, average surface temperature increases as the jet velocity is increased. This increase continues until nozzle velocity reaches a limiting value after which higher interaction between neighboring nozzles as well as higher ingress of ambient cold air decreases average surface temperature. For higher spacing between the nozzle and impinging surface, this shift occurs at a lower nozzle velocity.

Figure 4.16 shows time dependent heat transfer rate for different H/D ratios. As the distance between nozzle and impingement surface is increased, for the same velocity, longer time is required for the jet to reach the surface, during which mixing region and free flow regions of the jet continue to expand creating interference with the neighboring jets. At low H/D ratios, high reverse flow creates colder spots on the impingement surface. This results in extremely low values of time dependent heat transfer rate (integral value over the surface) for higher and lower H/D ratios. Optimum values of heat transfer rate are obtained at H/D ratios between 6 and 8.

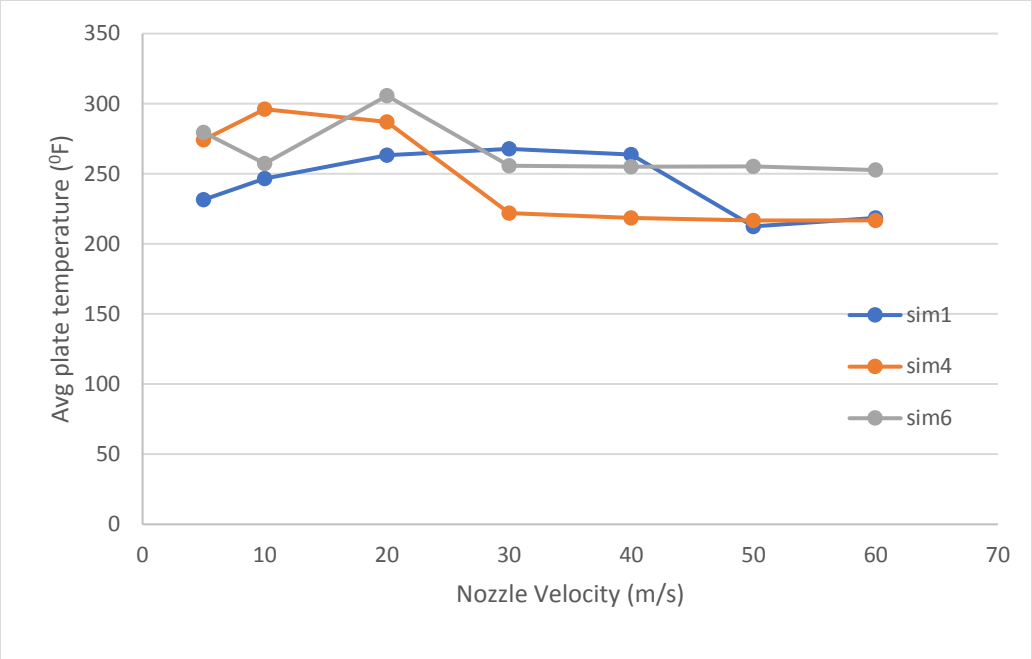

Figure 4.15: Average plate temperature for different H/D ratios

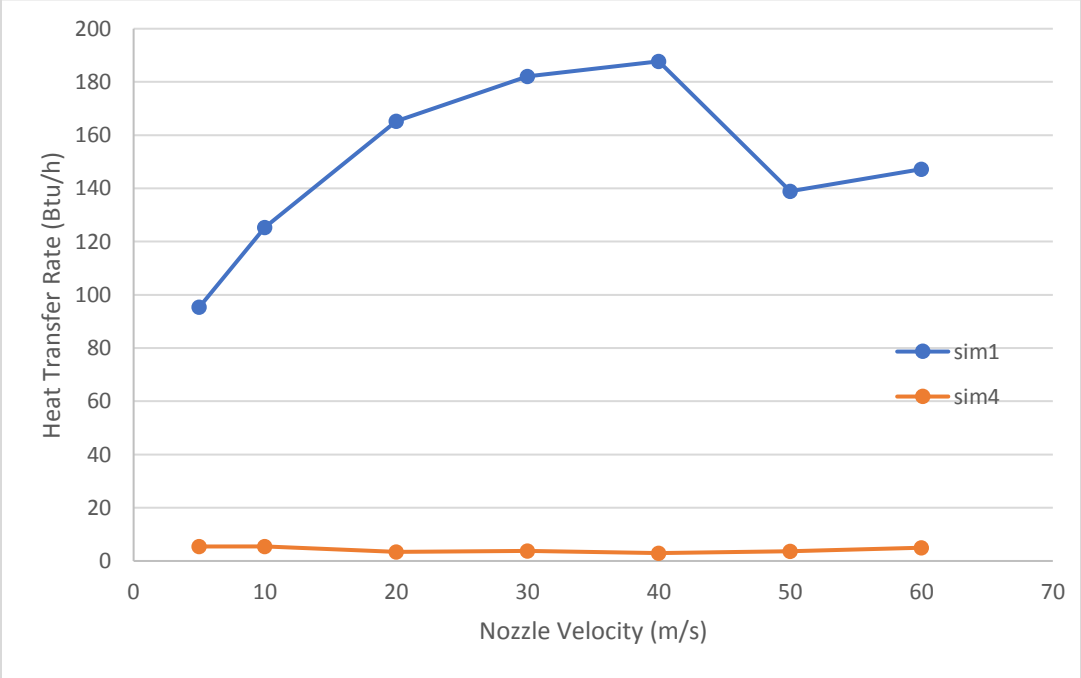

Figure 4.16: Heat transfer rate for different H/D ratios

4.3 Conclusions

Analysis and optimization of different controlling parameters during multi-jet air impingement shows how parameters such as Nozzle Velocity, H/D ratio and S/D ratio affect output parameters such as local and average and heat transfer coefficient, average impingement surface temperature and heat transfer rate. Highest values of heat transfer coefficient occur at stagnation point. The next higher peak occurs outside the boundaries of stagnation zone where air accelerates before it starts slowing down along the impingement surface. For three nozzle arrangements, air flow from the center jet, shifts the tips of neighboring jets away from the center jet. The effect is more pronounced at lower S/D ratios due to increased interaction with center jet. Higher S/D ratios result in higher local heat transfer coefficient values near stagnation point but the increased spacing between jets results in less coverage of the impingement surface reducing the average heat transfer coefficient over the impingement surface. Lower H/D ratios result in higher heat transfer coefficient peaks. The peaks for all three nozzles are more uniformed for H/D ratios between 6 and 8. For a fixed velocity, heat transfer coefficient values are directly proportional to nozzle diameter. For a fixed H/D and S/D ratio, heat transfer rate and average impingement surface temperature increases as the nozzle velocity increases until it reaches a limiting value. Further increase in nozzle velocity causes drop in heat transfer rate due to ingress of large amounts of cold ambient air in the control volume.

In the next chapter CFD analysis of a complete oven is performed. A number of key parameters are identified and the ones that have the most impact are varied to reach to an optimum configuration.

CHAPTER 5: CASE STUDY: SIMULATION OF CONVEYOR OVEN

The initial configuration of conveyor oven is designed in a 3D modelling software based on publicly available information and common industry knowledge. Through the process of optimization, a unique configuration is reached. The process to reach the optimum configuration and results of analysis are discussed in this chapter.

5.1 Conveyor Oven Construction and 3D Model

To analyze forced convection conveyor ovens, it is important to understand its basic structure and workings. Figure 5.1 below shows a typical countertop conveyor oven.

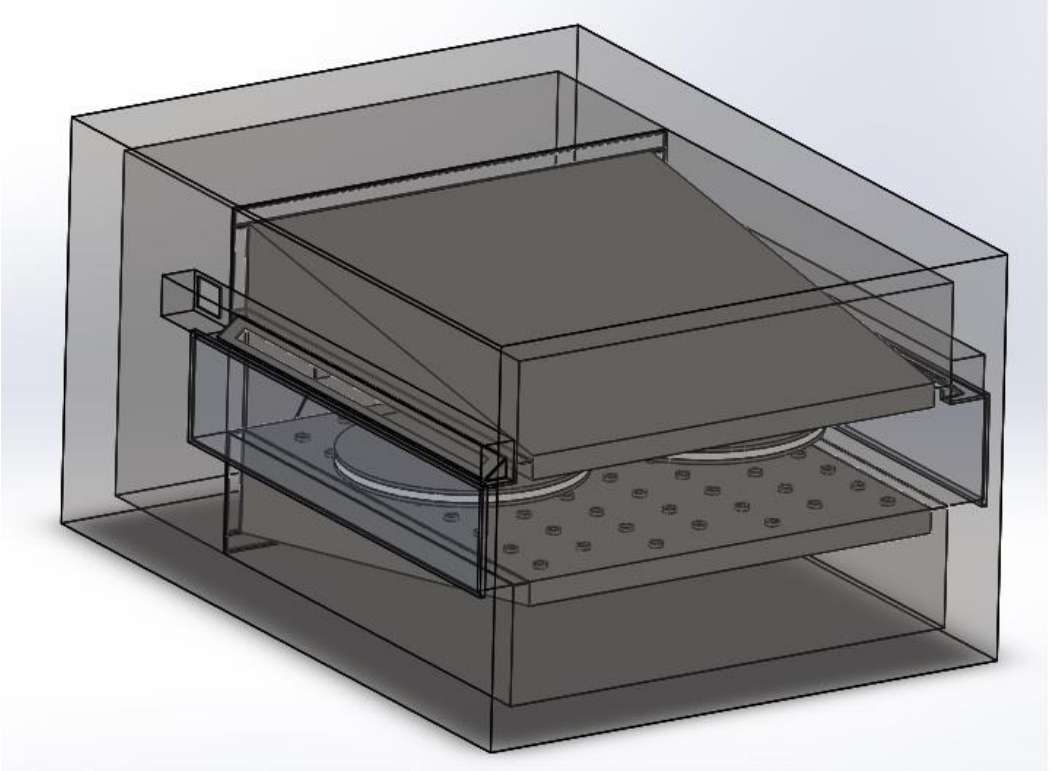

Figure 5.1: Conveyor oven 3D model

These ovens are used to cook variety of food from Pizzas to Pastas. Conveyor ovens are known to do job efficiently with shorter cook times and uniform cooking quality as compared to their traditional counterparts. Product to cook is fed on the conveyor belt either manually or with the help of robots. The belt drives the food through the oven where hot air is impinged on the food. Through careful planning of recipes and help from Engineers who design the ovens, the food is perfectly cooked as it exits the oven cavity. Even through conveyor ovens must be open on the sides to allow entry and exit of the food product, with careful design, an oven can be balanced to recirculate most of its air. Ingress of surrounding air lowers the temperature in the oven and affects its efficiency, hence air leakage is an important parameter when it comes to designing of the oven. A typical air impingement conveyor oven consists of several key components:

1) Oven Body: This is the outer shell of the oven. It acts as a housing for all oven components. Oven bodies are made of stainless steel sheet metal. Oven bodies are often cooled by recirculating cold air or insulated with heavy thermal insulation to avoid risk of burns and injury if someone touches the oven body when oven is operational
2) User Interface: A user interface panel can be found on the oven body usually in the area easily accessible by the user. Depending upon the model of the oven this panel can be a push button interface or a state-of-the-art touch screen interface. Important oven parameters such as conveyor speed and oven temperature can be varied via user interface. Newer technologies can be integrated in the oven which can show useful information on user interface such detecting when product enters and exist the oven, cleaning reminders and product count etc.

3) Conveyor belt: Conveyor belt moves the food in the oven from entry to exit. It is driven by a variable speed motor. In some ovens, the direction of belt is reversible allowing to easily configure entry and exit locations depending upon where the oven is installed.
4) Blower fan: This provides mechanism for air to circulate within the oven. Different types of fans ranging from radial to axial fans are used in the ovens depending upon the performance requirements.
5) Heater: Circulating air is heated before it enters the fan. In some oven configurations air heater can be found downstream of the fan air flow. Two common types of air heaters are used in impingement ovens a) Gas Heater: A flame is produced over a metal mesh heater using natural gas or propane. b) Electric heater: A metal rod is heated by passing a high voltage electric current. In both configurations one or more heaters are strategically placed to increase heat transfer to air flowing over it.
6) Fingers: Hot air from the fan is distributed to the oven cavity through a set of air passages called fingers. Depending upon size of oven, one or more fingers can be present inside the ovens. The shape of the finger and pattern of holes in the finger determines efficiency of the oven.
7) Return air ducts: Air impinged through holes in the finger must be returned to the fan for effective air circulation. This is accomplished by carefully designed return ducts that create an area of negative pressure which helps bringing the air back to the inlet of the fan. Unoptimized return air duct geometry can lead to unbalanced oven directly affecting energy consumption of the oven as well as quality of the food.

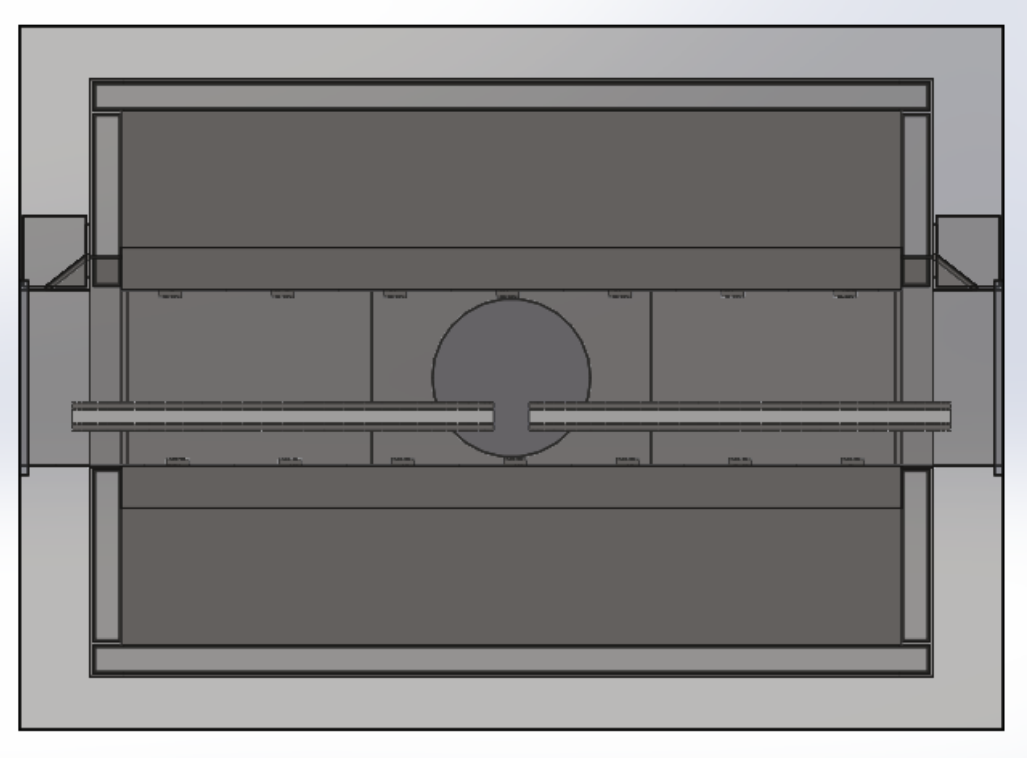

Figure 5.2: Oven front view

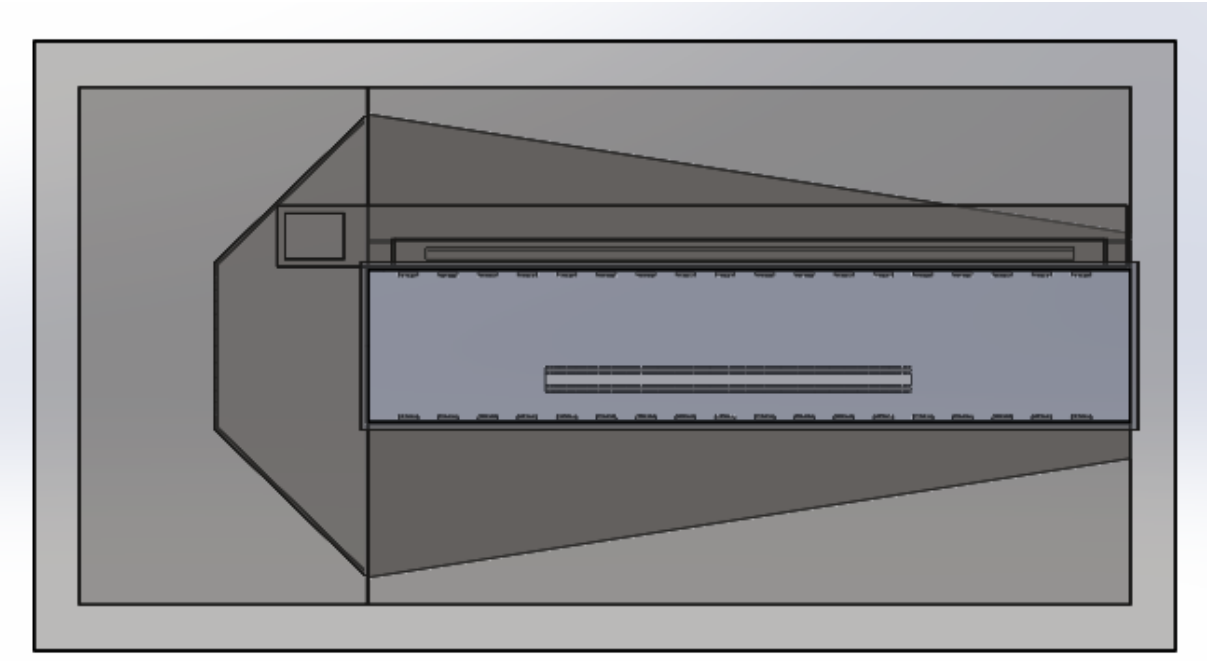

Figure 5.3: Oven side view

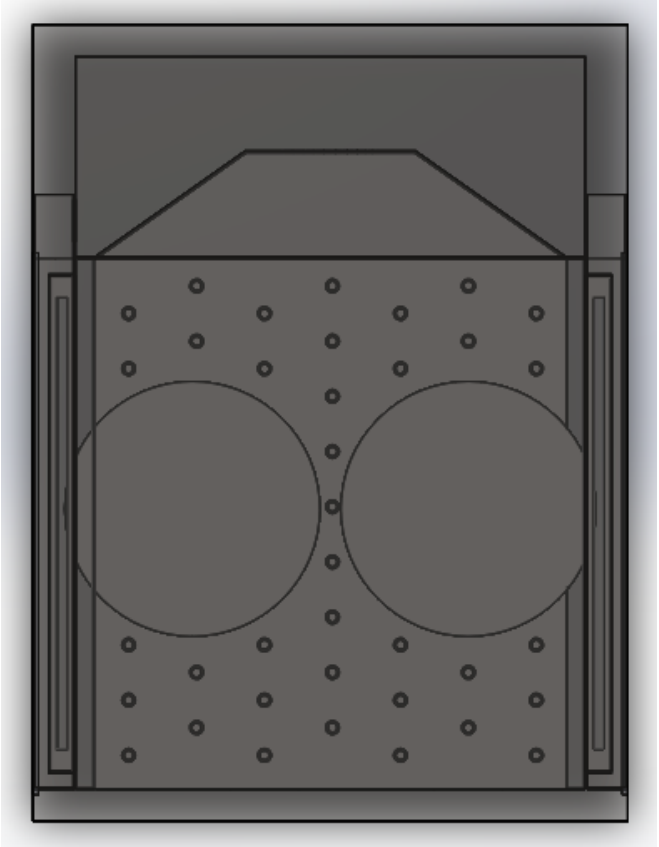

Figure 5.4: Oven top view

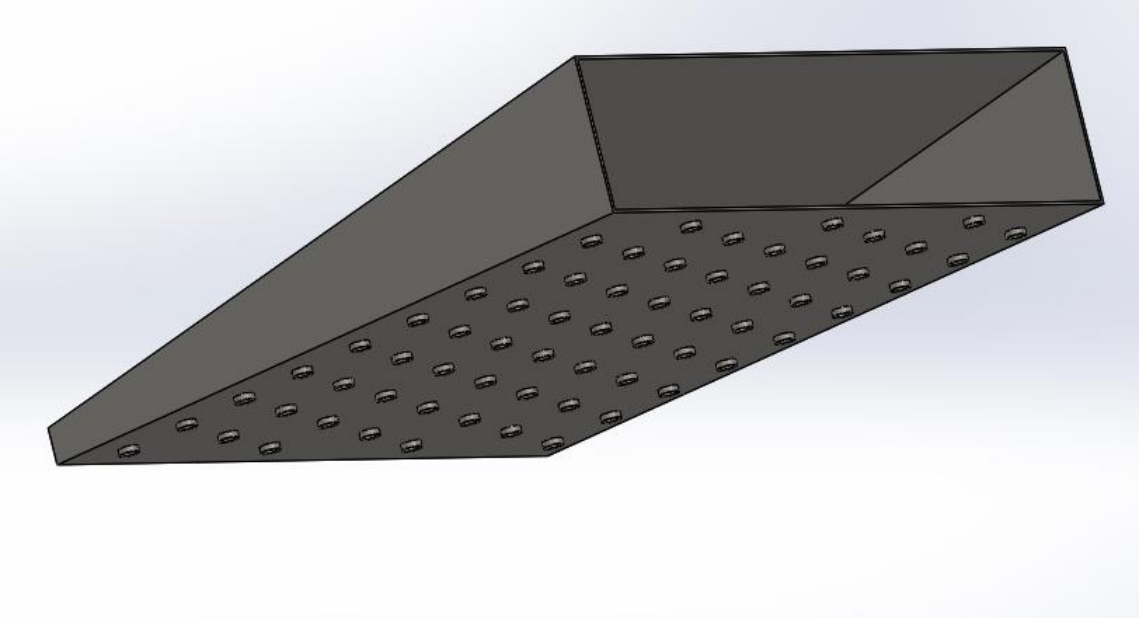

Figure 5.5: Oven finger

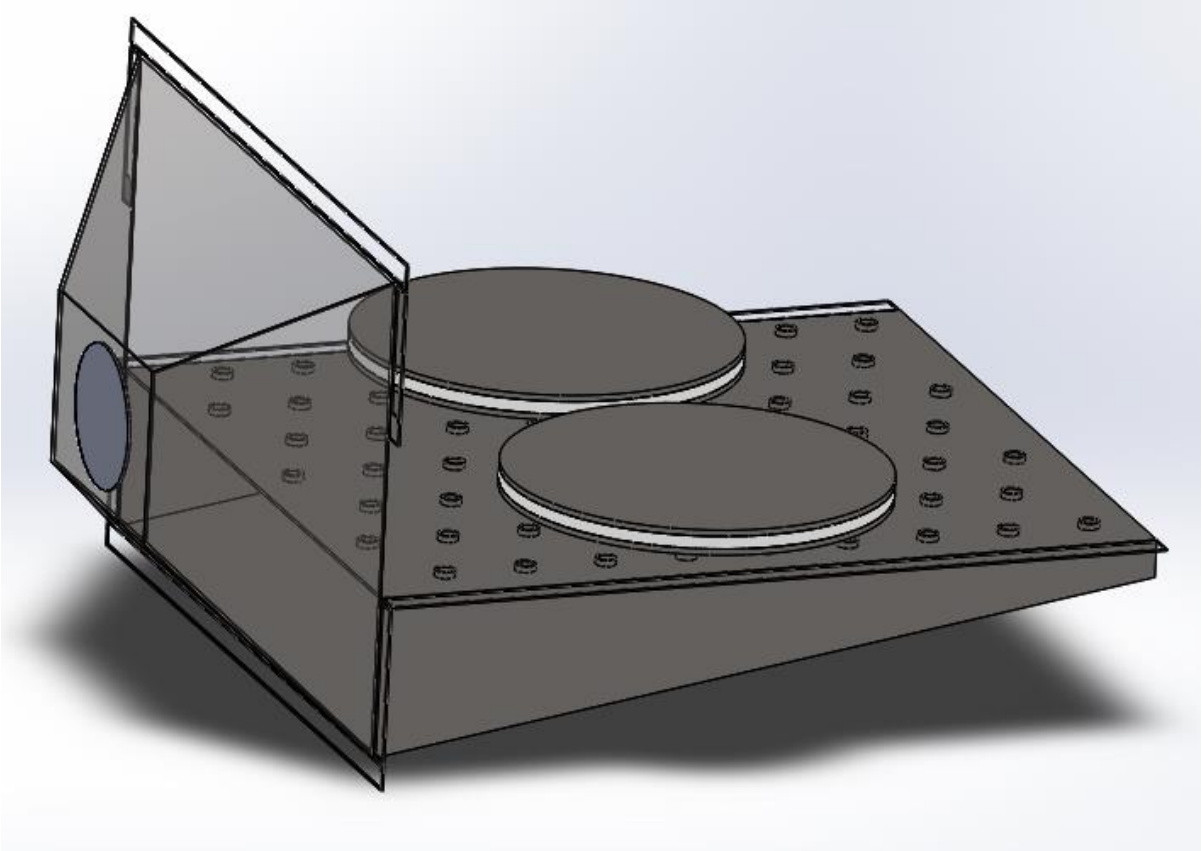

Figure 5.6: Fan blower cavity

Using air impingement conveyor ovens is one of the fastest methods to cook pizza. Total cooking time can be reduced by up to 60% while maintaining the quality using hot air impingement. Though widely used in pizza making Quick Service Restaurants (QSRs), a challenge remains to perfectly balance these ovens to produce quality results while reducing noise and energy costs. In Pizza ovens, conveyor belts are typically placed closer to bottom fingers as compared to top fingers. Cooking pizza requires about 30% more energy from the bottom of the pizza compared to top of the pizza. Top fingers are used to melt cheese and cook ingredients (toppings) on the pizza whereas bottom fingers which are closer to pizza are used to cook dough and create a harder bottom surface which acts as a support for soft dough above it. As the dough rises, the cheese melts in the dough creating a perfectly cooked pizza. Cooking

pizza in an unbalanced oven can severely affect its quality. Too much heat at the bottom makes the dough too hard creating unwanted crispiness. Uneven jet velocities can cause cold/hot spots on pizza. Cooking with non-uniform air temperature distribution can cause layer of cheese to melt and quickly solidify creating a barrier for rest of the ingredients under the layer. A thorough methodical investigation of controlling parameters is necessary to design a balanced oven.

Due to large number of controlling parameters affecting the air and temperature distribution, it is expensive in terms of both time and material to perform "design of experiments" on a conveyor oven. Computer simulation can be used to narrow down the set of variables. Once an optimum configuration is determined a full prototype can be built to validate the improvements made to the oven. During this research, a steady state Computational Fluid Dynamics (CFD) simulation was performed on an air impingement conveyor oven using professional version of Solidwork's Flow Simulation package. A mesh independence study was carried out using quadrilateral mesh elements. Two 12" targets simulating typical medium size pizzas were placed on a conveyor. Entry and exit points on the left and right side of the oven were open to atmosphere. Heated air was impinged on targets via top and bottom fingers through a series of holes. A detailed study of air circulation patterns, jet interactions, heat transfer coefficients on target surface as well as air leakage to and from the oven was performed. Results from the simulations can be used to establish design guidelines for any air impingement conveyor oven.

5.2 Configurations

To reach an optimum configuration, a structured approach was used. Based on existing literature and common industry knowledge, a list of controlling parameters was developed. The list included:

1) Oven Type: Counter top Vs Free Standing
2) Oven Size: Small (upto 30” wide), Medium (upto 42” wide), Large (24” wide and up)
3) Plenum (finger) geometry: Square Vs Tapered
4) Cooking profile in the oven: Variable vs Uniform
5) Type of fan: Radial Vs Axial
6) Number of fans
7) Convective and radiative losses from the oven
8) Placement of heaters
9) Number of fingers
10) Geometry within a finger: Air deflectors and guide vanes
11) Diameter (D) of impingement nozzle
12) Number of impingement nozzles
13) Distance between nozzle and impingement surface (H)
14) Spacing between adjacent nozzles (S)
15) Pattern of nozzles in the finger
16) Type of Nozzles: Extruded holes Vs non-extruded holes
17) Return air duct design
18) Fan CFM

19) Air curtain technology: Blowing a curtain of air over the entry and exit points to keep oven air from escaping
20) Air filter placement and pressure drop across the filter
21) Conveyor belt placement
22) Conveyor belt speed and direction
23) Amount of product used in simulation

Due to an extensive nature of the list and number of permutations and combinations of all parameters being extremely high, a separate list of high impact parameters was created. Some parameters were combined to form non-dimensional parameters such as Height (H) over Diameter (D) ratio. The rest of parameters were assigned a fixed value. The parameters that were assigned a fixed value are listed below:

1) Oven Type: Counter top
2) Oven Size: Small (Cavity 28" wide x 24" deep)
3) Cooking profile in the oven: Uniform
4) Type of fan: Axial
5) Number of fans: One
6) Convective & Radiative losses from hot oven surfaces to ambient were ignored for this simulation. (In the industry, these losses are minimized by use of high performance insulation or blowing cold air on inside surfaces of oven skin)
7) Placement of heaters: Upstream of fan air flow
8) Number of fingers: One top finger and one bottom finger

9) Geometry within finger: Larger oven require guide vanes to direct flow of air within the finger. Since a smaller oven was analyzed, a uniform flow was obtained without the use of guide vanes
10) Pattern of nozzles in the finger: A stacked nozzle pattern was used to ensure maximum coverage of the impingement surface
11) Air curtain technology: Air curtain technology was not used in simulation
12) Air filter placement and pressure drop across the air filter was ignored
13) Conveyor belt placement: Conveyor belt was placed so that bottom of the target was 1" away from the bottom finger. This enabled top surface of the target to be 3.2" away from the top finger
14) Conveyor belt speed & direction: As steady state analysis was carried out. Belt speed and direction were out of scope of this investigation and thus ignored.
15) Amount of product used in simulation: Two 12" diameter targets representing two medium sized pizzas were placed side by side from entry to the exit of the oven.

Following table shows simulations performed on different configurations by varying high impact parameters. The values chosen for high impact parameters were based on existing literature, industry practices, known manufacturing limitations and physical limitations of the equipment. These high impact parameters were further sorted depending upon their perceived impact on oven performance. For example, plenum (finger) geometry was identified as the most important parameter and hence was put on the top of the list to be varied. Variations within each high impact parameter were carefully studied by obtaining results of the simulations. Based on heat transfer coefficient, average heat rate, average heat flux over the target surface and leakage air entering the oven, an optimum variant of the parameter was chosen. This optimum variant

was kept constant and next high impact parameter was varied. This process was repeated until all high impact parameters were studied. When a final optimized solution was reached and compared to the starting configuration, improvement in average heat transfer coefficient was 22.7%, improvement in average surface heat flux was 24.7% and improvement in leakage air mass flow rate was 59.1%.

Table 5.1: Oven configurations

Config #	plenum geometry	extruded holes	H/D	Spacing (inches)	return duct geometry	CFM
1	squared	no exrtude	7	3.2	open	350
2	tapered	no extrude	7	3.2	open	350
3	optimum	extrude 0.187	7	3.2	open	350
4	optimum	extrude 0.25	7	3.2	open	350
5	optimum	extrude 0.375	7	3.2	open	350
6	optimum	optimum extrude	4	3.2	open	350
7	optimum	optimum extrude	5	3.2	open	350
8	optimum	optimum extrude	6	3.2	open	350
9	optimum	optimum extrude	7	3.2	open	350
10	optimum	optimum extrude	8	3.2	open	350
11	optimum	optimum extrude	9	3.2	open	350
12	optimum	optimum extrude	10	3.2	open	350
13	optimum	optimum extrude	optimum H/D	2	open	350
14	optimum	optimum extrude	optimum H/D	2.5	open	350
15	optimum	optimum extrude	optimum H/D	3.2	open	350

Table 5.1 (Continued)

16	optimum	optimum extrude	optimum H/D	3.8	open	350
17	optimum	optimum extrude	optimum H/D	4.4	open	350
18	optimum	optimum extrude	optimum H/D	optimum spacing	open	350
19	optimum	optimum extrude	optimum H/D	optimum spacing	close at the back (15%)	350
20	optimum	optimum extrude	optimum H/D	optimum spacing	close more at back (30%)	350
21	optimum	optimum extrude	optimum H/D	optimum spacing	graduated holes pattern #1	350
22	optimum	optimum extrude	optimum H/D	optimum spacing	graduated holes pattern #2	350
23	optimum	optimum extrude	optimum H/D	optimum spacing	optimum return	350
24	optimum	optimum extrude	optimum H/D	optimum spacing	optimum return	450
25	optimum	optimum extrude	optimum H/D	optimum spacing	optimum return	550
28	optimum	optimum extrude	optimum H/D	optimum spacing	optimum return	Optimum CFM

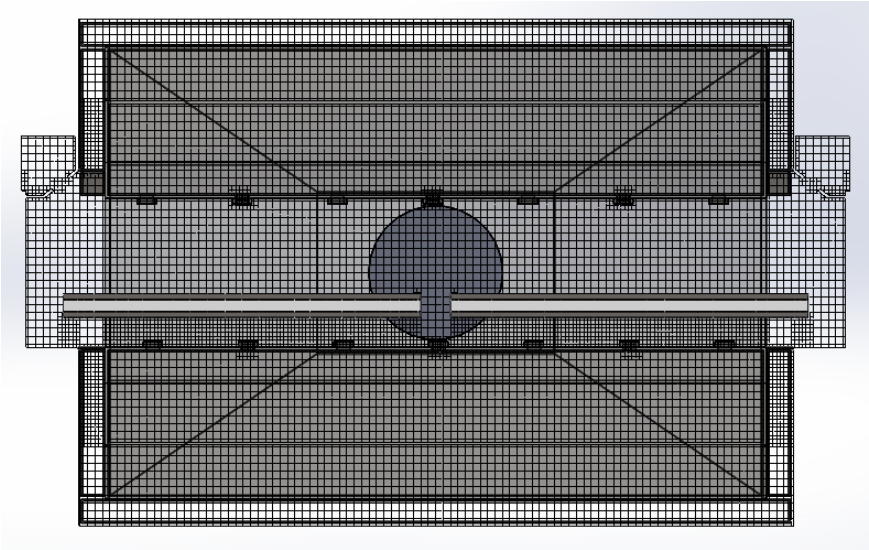

Figure 5.7: Mesh front view

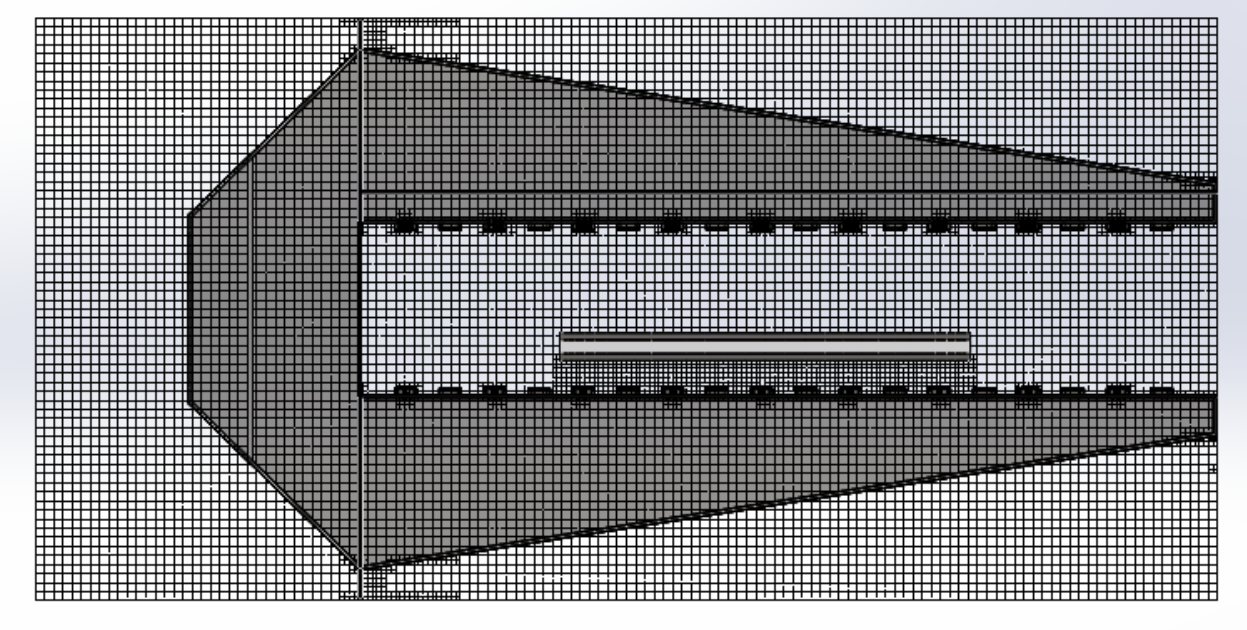

Figure 5.8: Mesh side view

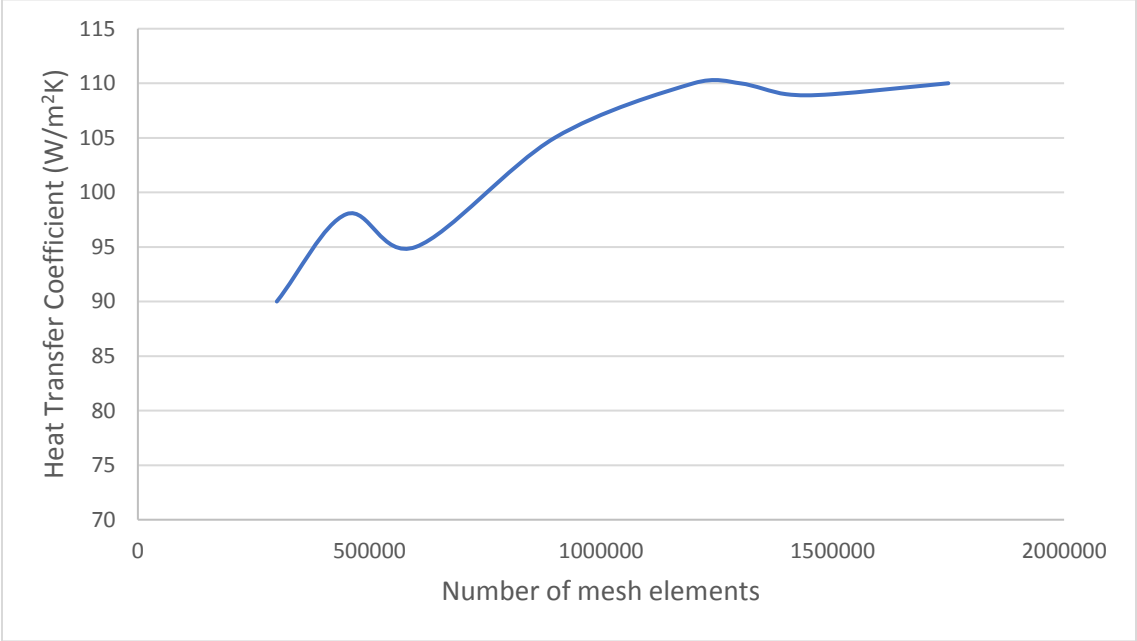

Figure 5.9: Mesh independence study

Figure 5.9 shows heat transfer coefficient on top surface of left target. Mesh independence study was carried out to determine optimum mesh size. Total number of fluid mesh elements were varied starting from 30,000 elements up to 1.75 million elements. It was

found that variation in results was less than 2% as mesh size was increased beyond 1.3 million elements. To optimize run-time for simulations while maintaining results accuracy, mesh size of ~1.3 million elements was chosen for all simulations

5.2.1 Square Vs Tapered Fingers

Maintaining air balance across the entire cavity of the oven is essential for cooking food evenly. In poorly balanced ovens, one might get different cooking results depending upon where the food is placed inside the oven. This directly affects the quality of food. Shape of the fingers is an essential parameter in obtaining a balanced airflow.

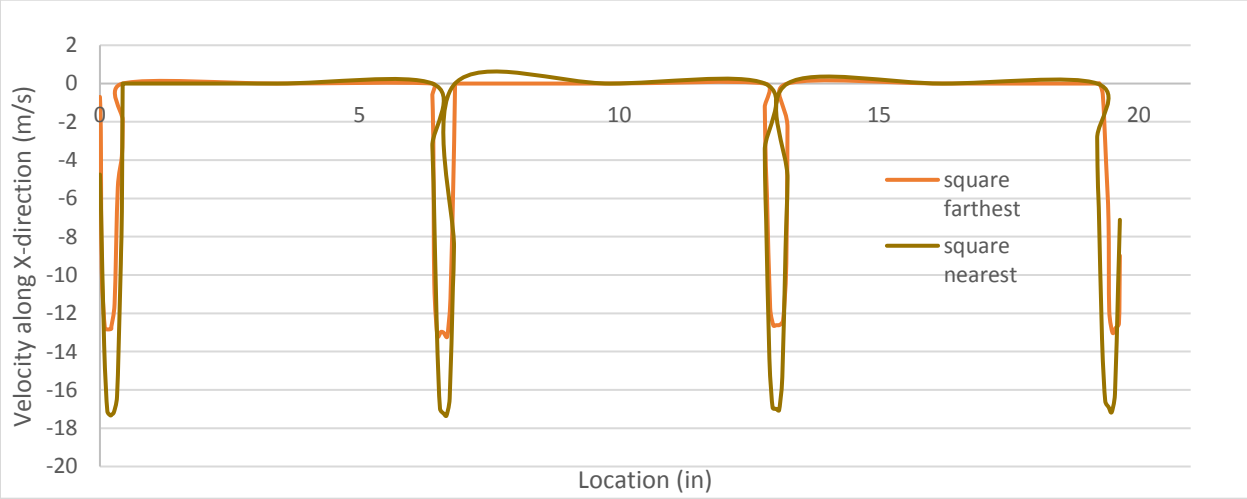

Figure 5.10: Velocity degradation in square fingers

Figure 5.10 shows velocity degradation in square fingers along x-axis taken along the lines parallel to front face of the oven. The readings are taken at the surface of the finger. Two different locations are studied viz. near the fan and farthest from the fan. It can be clearly seen that the air velocity coming out of impingement holes decreases as the distance from the fan is increased. This results in uneven velocity distribution throughout the oven. Uneven velocity distribution causes uneven heat transfer at different parts of the oven which is highly undesirable. One of the ways to address the problem of decreasing velocity in the finger away from fan is to

gradually decease the cross-sectional area that air must travel through inside the finger. The decreasing cross-sectional area helps to maintain uniform air velocity inside the finger. This is illustrated by graph in figure 5.11b. The graph shows air velocity in tapered fingers along x-axis for the lines parallel to front face of the oven. The air velocity is uniform throughout the oven resulting in uniform heat transfer.

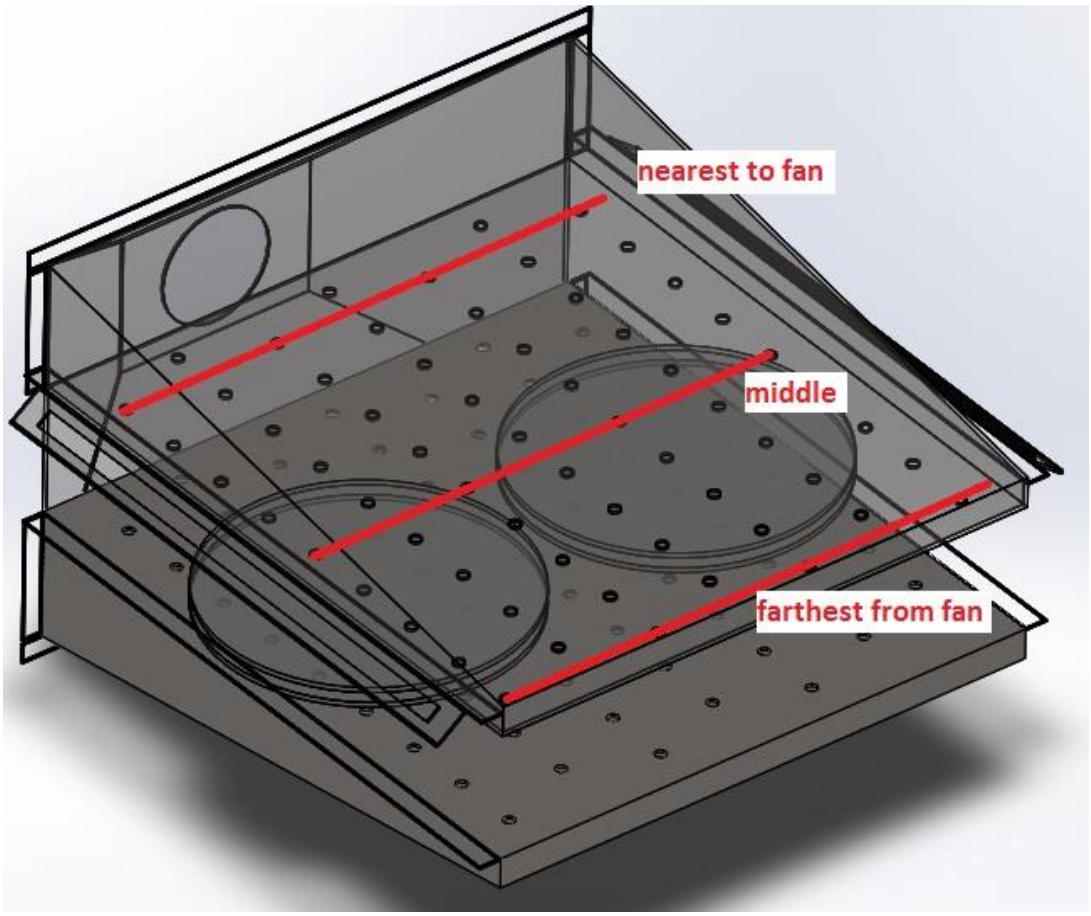

Figure 5.11a: Lines showing location of velocity readings for tapered fingers

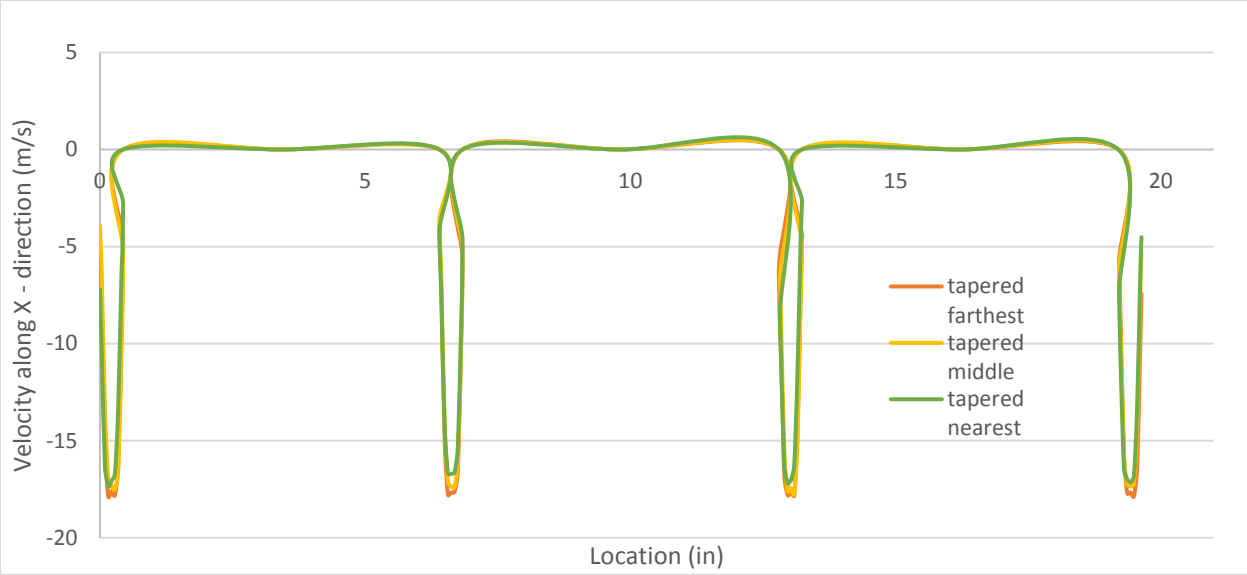

Figure 5.11b: Velocity degradation in tapered fingers

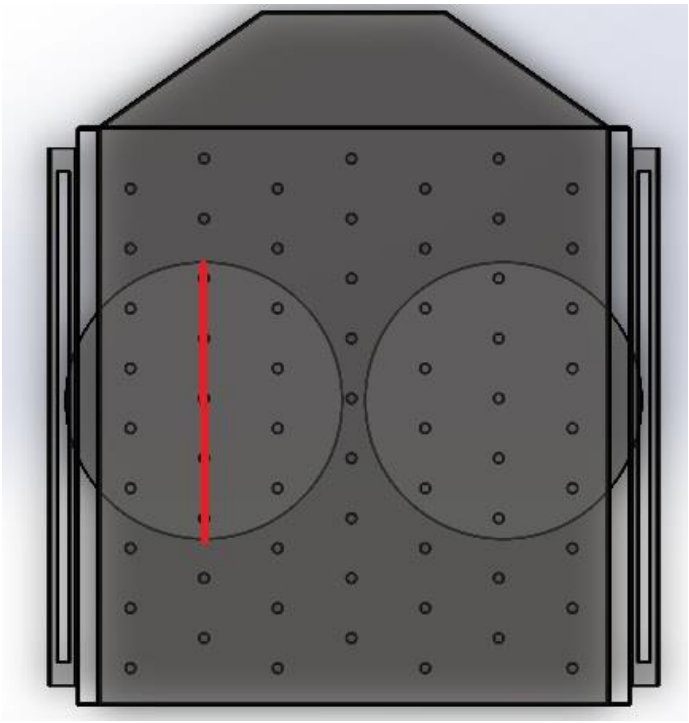

Figure 5.12a: Line showing location of heat transfer coefficient readings for square and tapered fingers

Figure 5.12b shows graph of heat transfer coefficient along the line starting from nearest to farthest from the fan. The heat transfer coefficient is calculated on top of the left-hand side

target. The decrease in heat transfer coefficient as one moves from nearest to farthest from the fan is clearly visible for square fingers. For tapered fingers the heat transfer coefficient distribution is much more uniform.

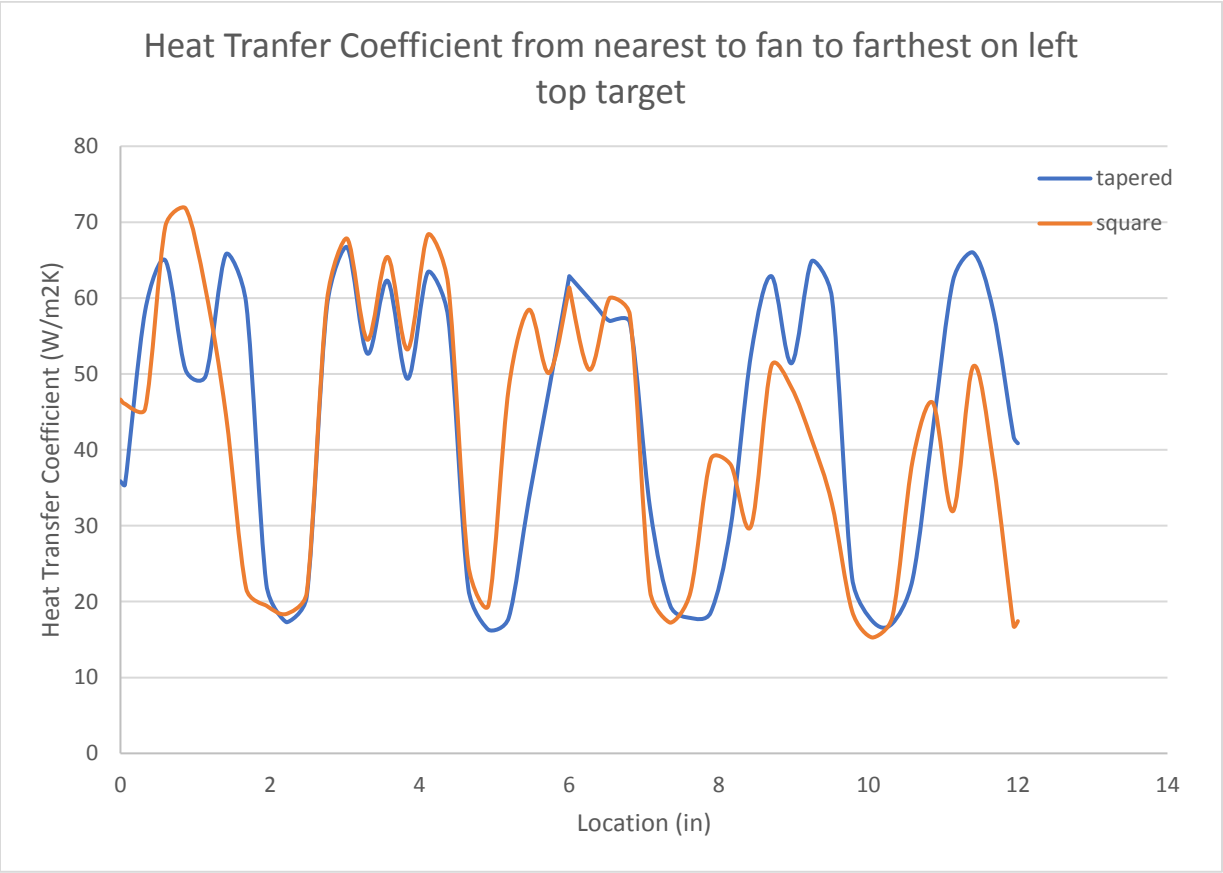

Figure 5.12b: Heat transfer coefficient for tapered vs square fingers

5.2.2 Extruded Vs Non-extruded Holes

Heat transfer in multi-nozzle configuration depends greatly on interaction between neighboring nozzles. The shape of the potential core of the jet is important for achieving high values of heat transfer. As shown in Figure 5.14, keeping all other parameters the same, fingers with extruded holes show higher heat transfer rates as compared to fingers with non-extruded holes. Extruded holes help better direct the jet towards impingement surface reducing the interaction between neighboring jets. Process of manufacturing fingers with extruded holes can

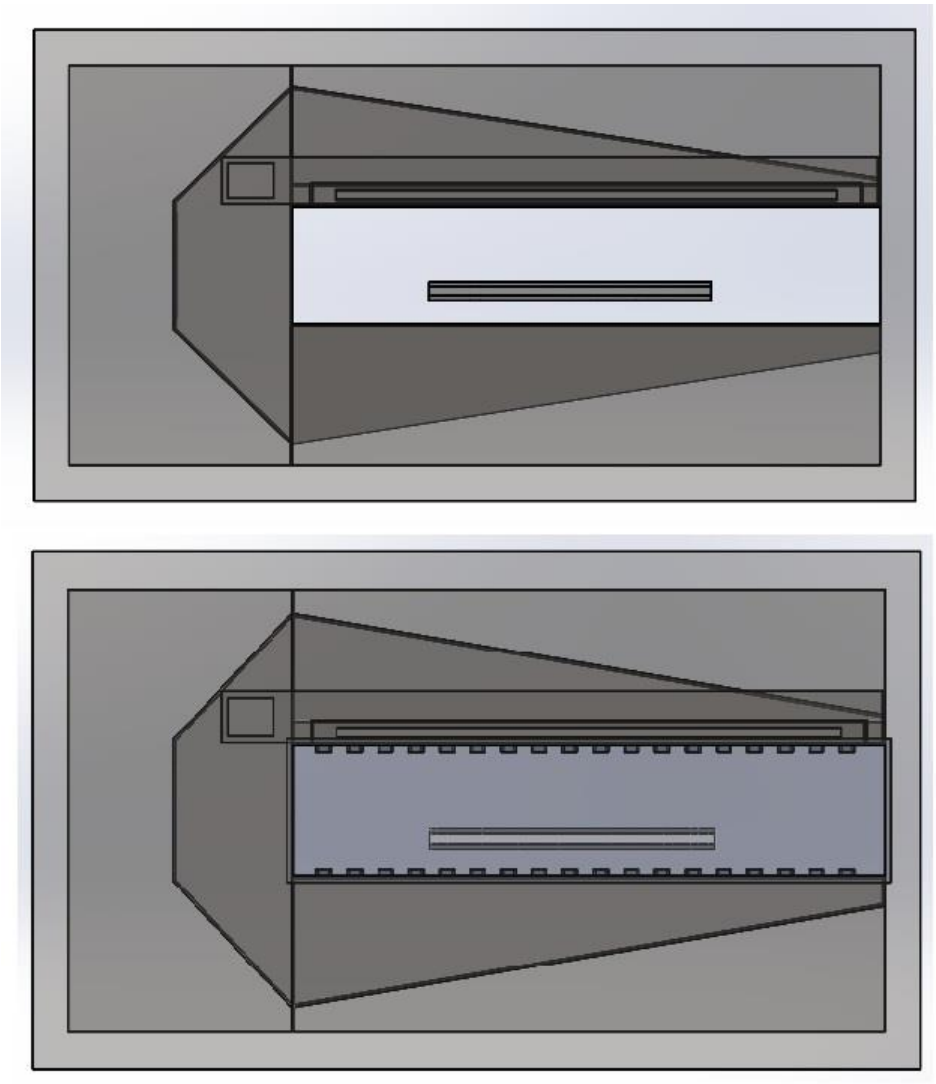

Figure 5.13: Oven side view showing non-extruded vs extruded finger holes

be automated using an oversized die that is hydraulically pressed upon the center of the hole. This causes material around the hole to be extruded in the direction of the motion of the die creating an extruded surface away from the surface of the finger. Hydraulic pressure and diameter of the die can be adjusted to control the length of extrusion. Simulations were performed with different extrusion lengths to optimize heat transfer. Average surface heat flux and average heat transfer rates were obtained for top surface of the left-hand side target. Figure 5.15 shows high rates of heat transfer and surface heat flux for extrusion length of 0.25”

(Configuration 4). As the extrusion length is increased beyond 0.25”, the jets become more concentrated. Local heat transfer coefficient is increased but less area of target is covered thus reducing average heat transfer rate and surface heat flux over the entire surface.

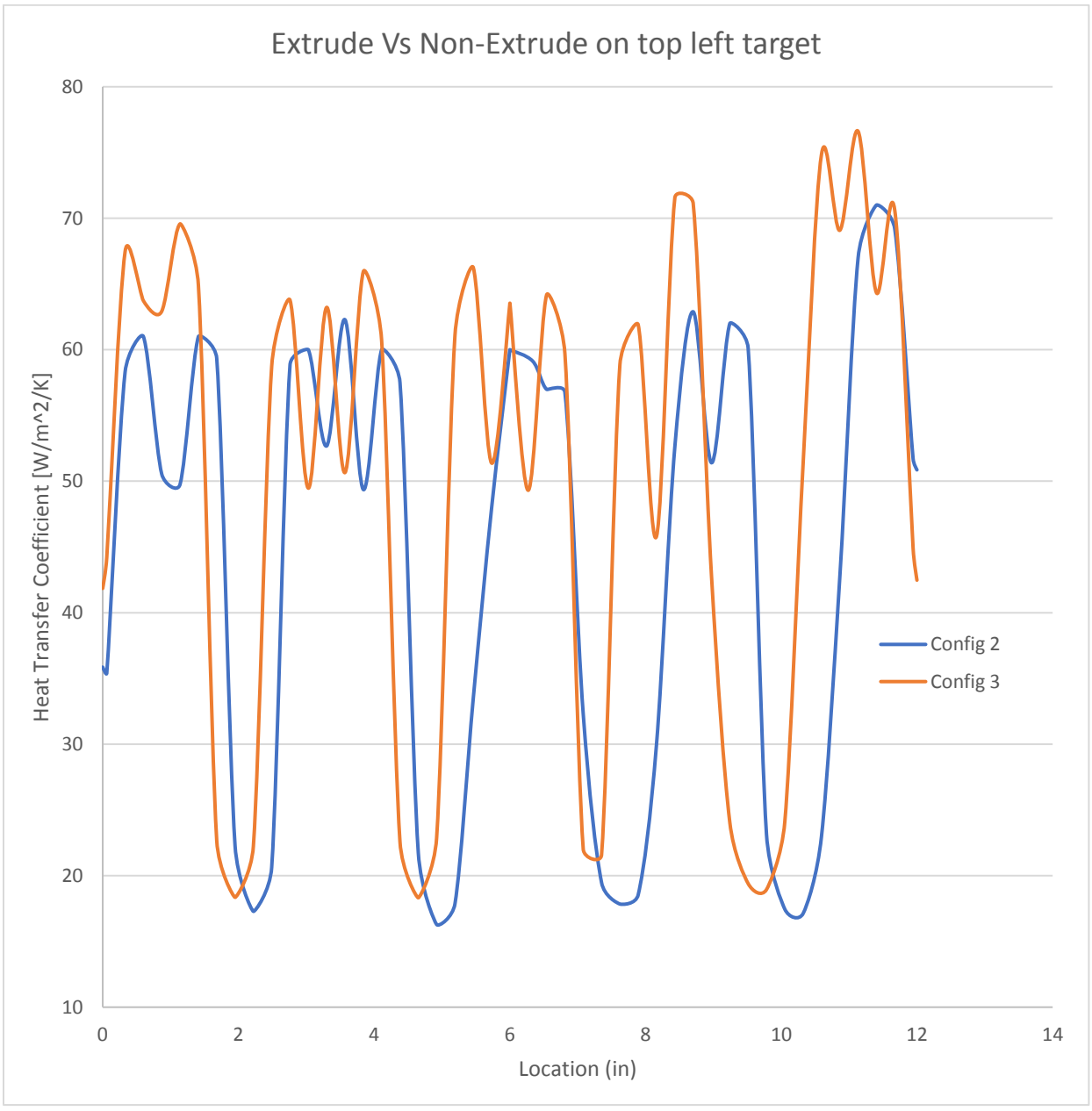

Figure 5.14: Heat transfer coefficients for extruded vs non-extruded holes

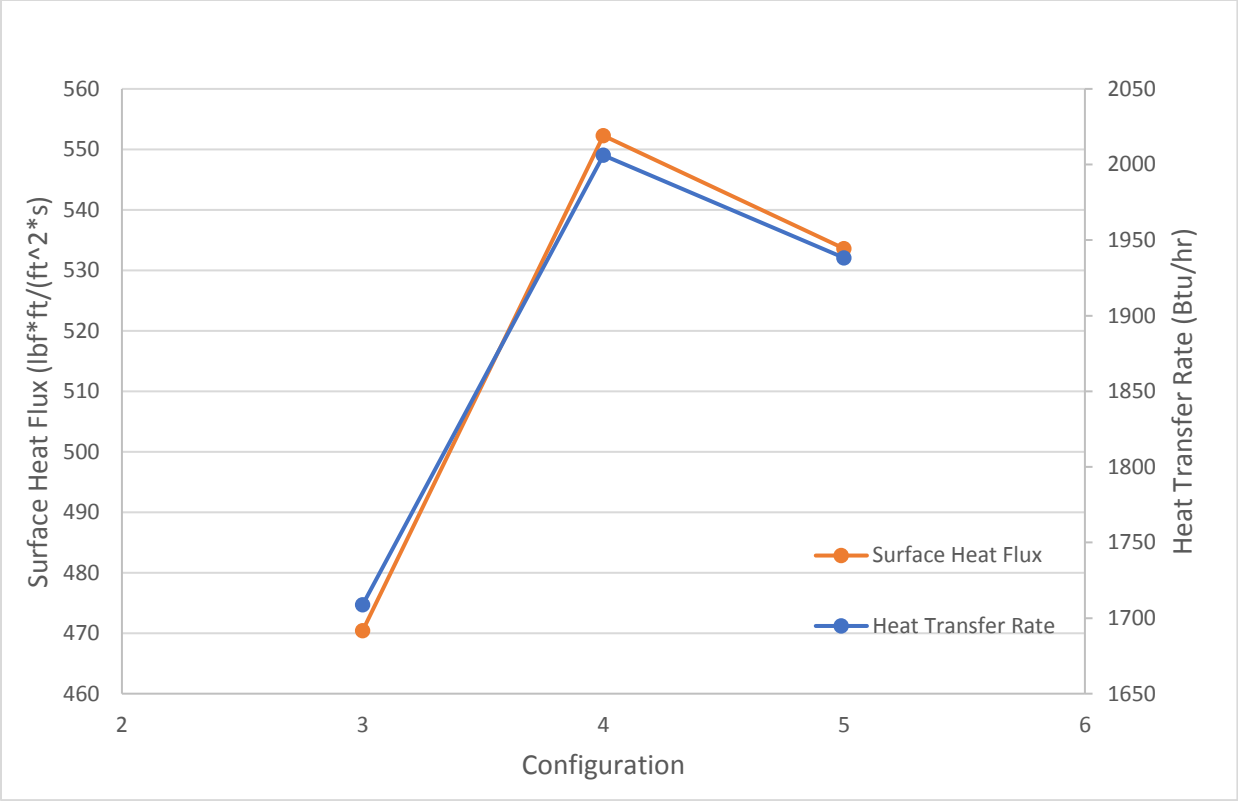

Figure 5.15: Extrude optimization

5.2.3 H/D Optimization

H/D ratio is one of the most important parameters when it comes to analyzing multiple jet impingement. As distance between nozzle and impingement surface increases, heat transfer coefficient decreases. Lower values of H can theoretically increase heat transfer coefficient but practically height of cooking product placed under the nozzle dictates minimum values of H. Diameter of jet has equal importance when it comes to heat transfer and interaction with neighboring jets. For a fixed spacing between the holes, jets coming from smaller holes do not cover sufficient area on the impingement surface lowering the average values of heat transfer over the entire surface. For the same spacing between the holes, jets coming from larger diameter holes have high degree of interaction between neighboring jets which adversely affects heat transfer coefficient. Along with these parameters, air leakage in and out of oven is equally

important. Since, conveyor ovens are open from the sides where product enter and exists the oven, cold air ingestion from ambient to a working hot oven adversely affects efficiency of the oven. Optimum configuration is chosen based on combined effects of heat transfer and leakage air. Figure 5.16 shows comparison between different configurations based on heat transfer rate, average surface heat flux and leakage air mass flow rate.

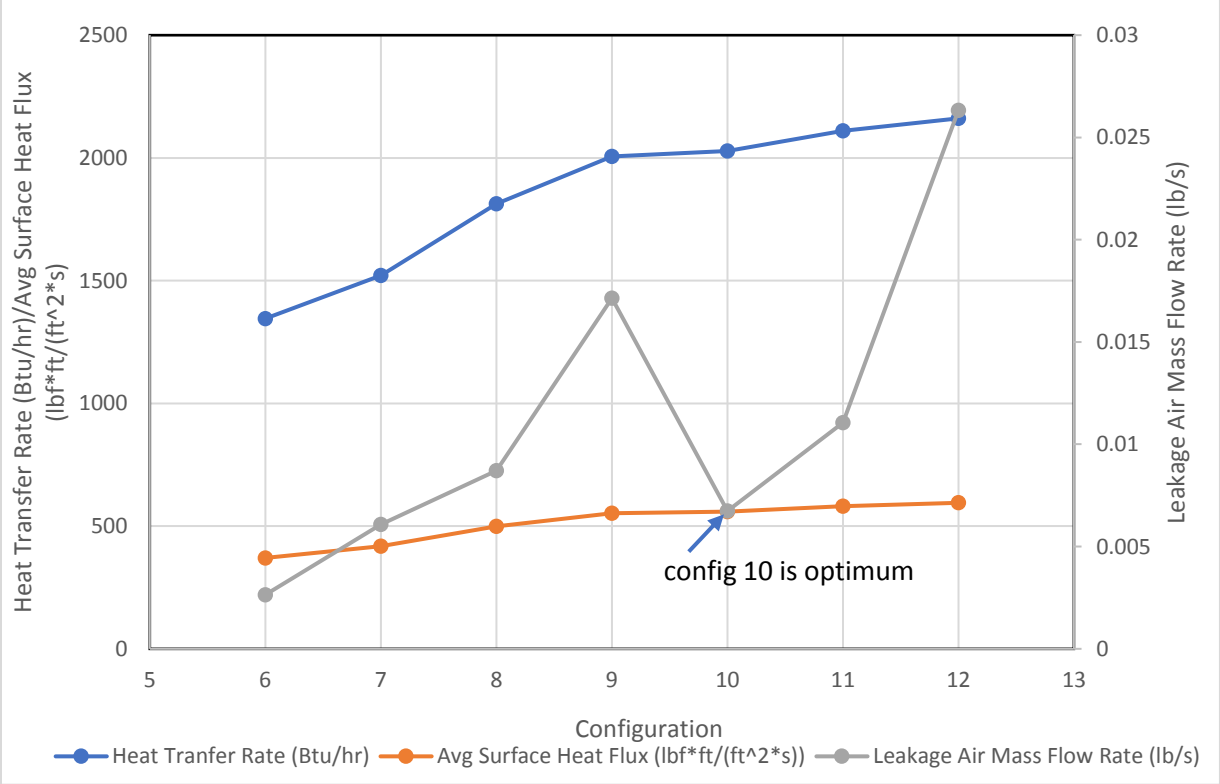

Figure 5.16: H/D optimization

5.2.4 S/D Optimization

A ratio of hole spacing to diameter of hole is another important parameter for designing efficient ovens. There is a range of S/D values where heat transfer is optimized. Smaller values of S/D indicate that the jets are closely packed together. This might increase interaction between neighboring jets increasing cross flow and adversely affecting the heat transfer process. Higher values of S/D indicate that jets are too far apart reducing the total impact area of impingement

reducing the overall heat transfer to the target. Simulations are run with different S/D ratios to find optimum values of heat transfer. Heat transfer rate, surface heat flux and total leakage is also analyzed. Figure 5.17 shows optimum configuration of S/D based on maximum values of heat transfer rate and surface heat flux.

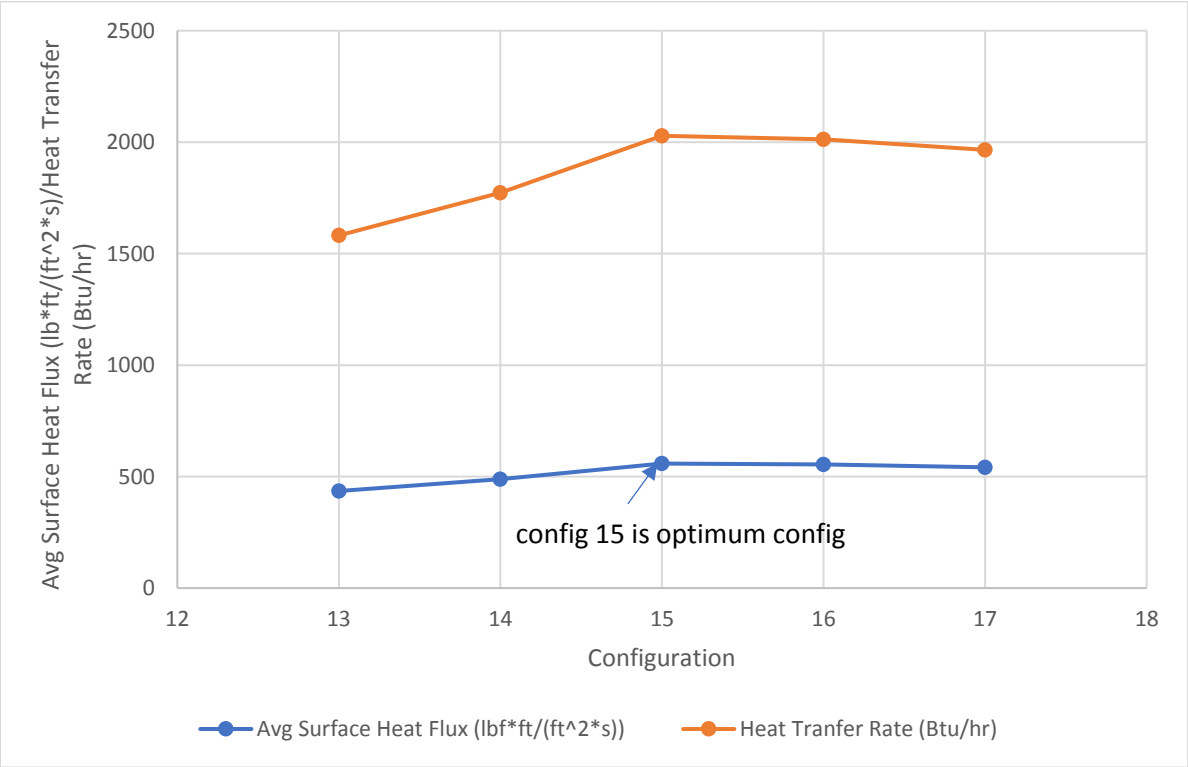

Figure 5.17: S/D optimization

5.2.5 Return Geometry Optimization

Air balance in conveyor oven is crucial to the efficiency of the oven. As ambient cold air enters the oven, it reduces the temperature of the existing hot air in the oven cavity. Since conveyor ovens must be open at both ends for entry and exit of the food, keeping hot air inside the oven becomes more challenging. Return geometry must be carefully designed so that amount of air entering and exiting oven is minimized. In the following set of simulations, different return geometries are analyzed to optimize ambient air leakage. Figure 5.18b shows lowest ambient air leakage rate for configuration 20. This is chosen as optimized configuration for return geometry.

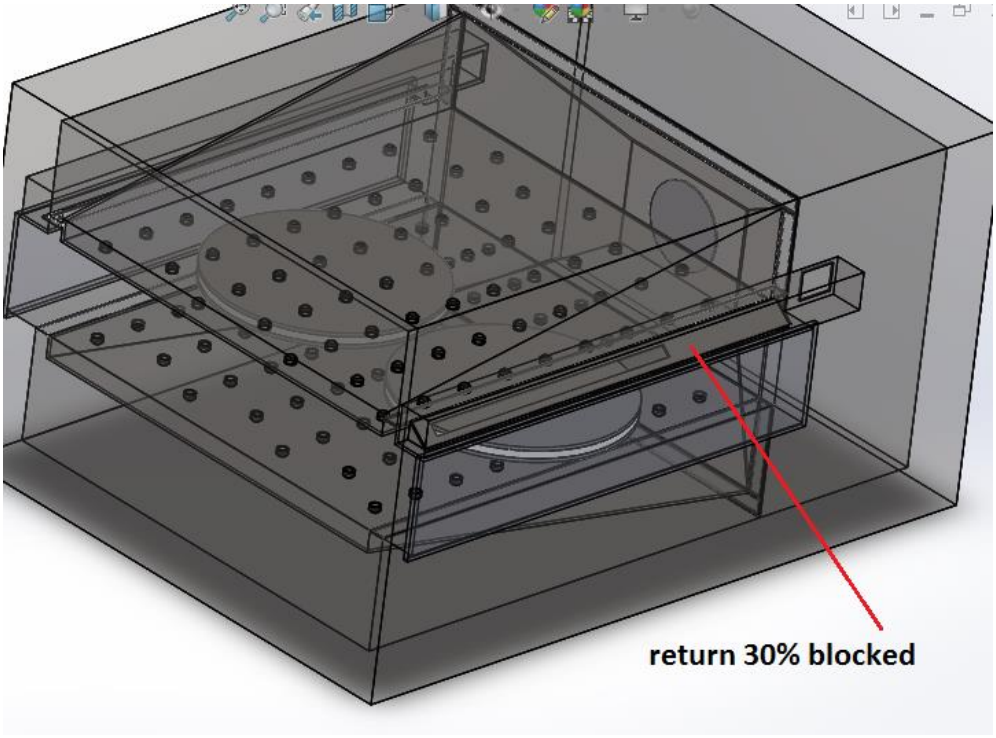

Figure 5.18a: Oven view showing return geometry

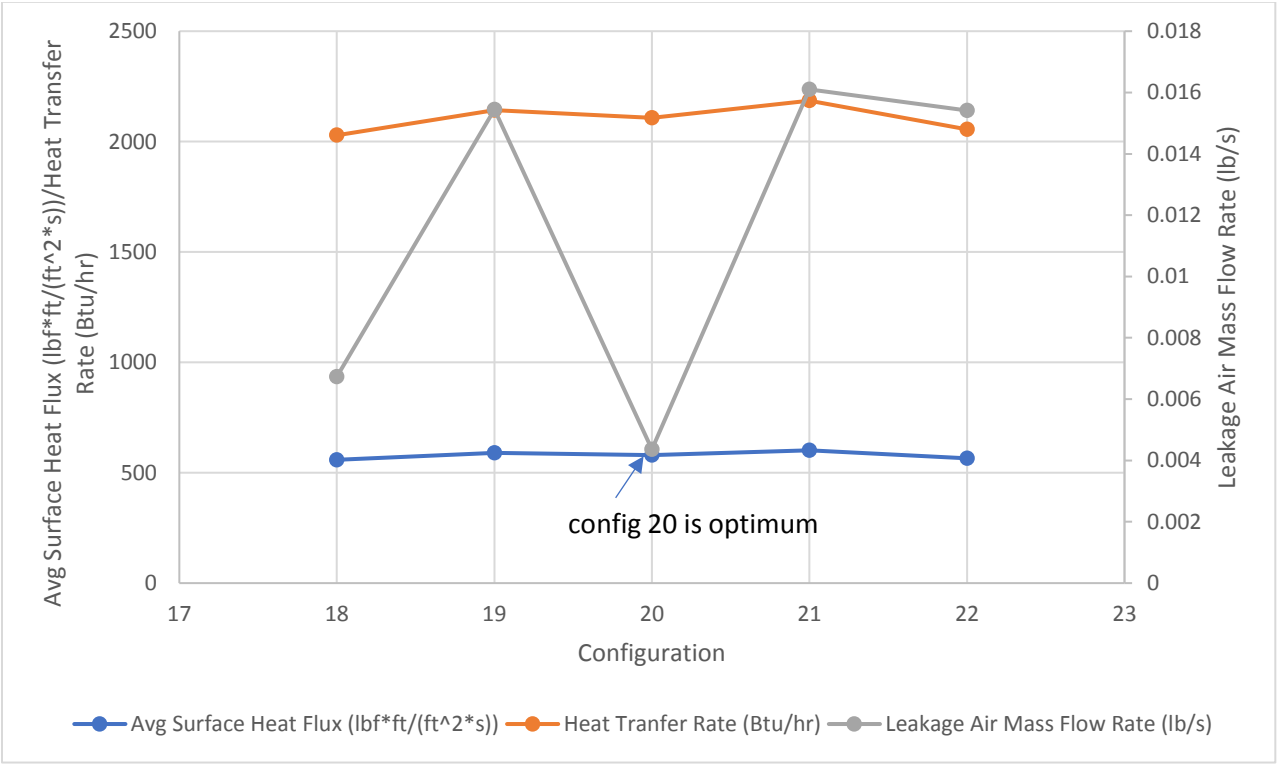

Figure 5.18b: Return configuration optimization

5.2.6 CFM Optimization

For most of analyses in this research an oven with 350 CFM fan is used. As shown in figure 5.19, heat transfer coefficient values are seen to be increasing with higher CFM. However, there are practical limitations for higher CFM fans. Higher volumetric air flow demands bigger air heating system which may turn out to be economically non-feasible for a particular size of the oven. Higher CFM also poses oven air balancing challenges with increased static air pressure inside the fingers. Finally, food particles can become airborne as higher CFM results in higher nozzle velocities. Due to these reasons, CFM optimization is highly subjective and depends greatly on type of food product being cooked.

Figure 5.19 shows velocity cut plot from the left side of the oven. It shows that if the food product does not take up the entire oven the jets with no product under them create a disturbance in air pattern which could affect heat transfer from the jets at the extreme end of the product

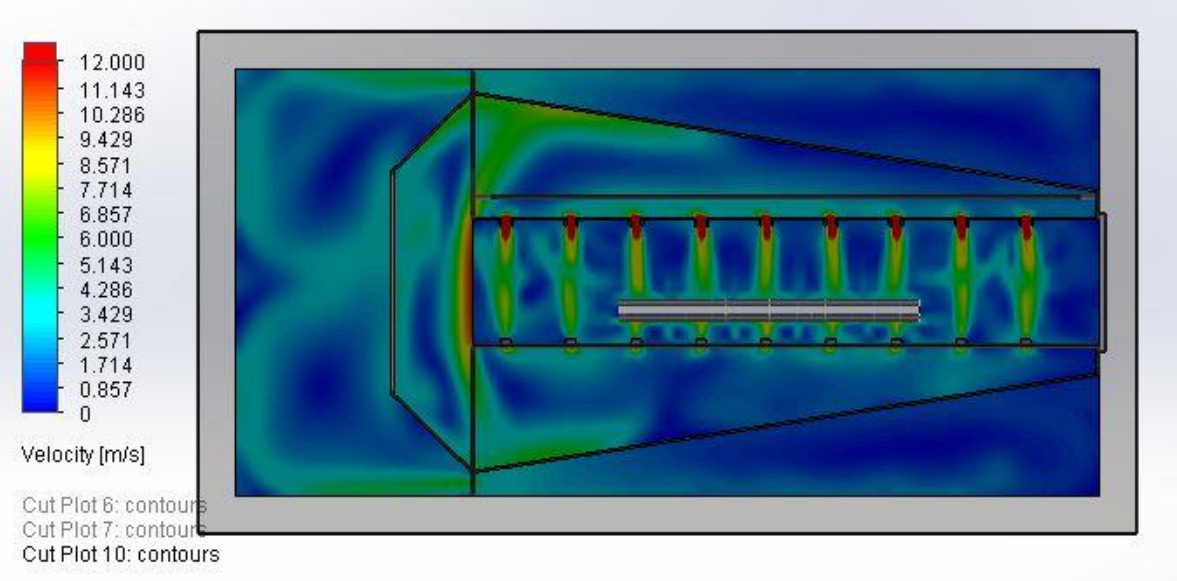

Figure 5.19: Velocity plot of side view of the oven

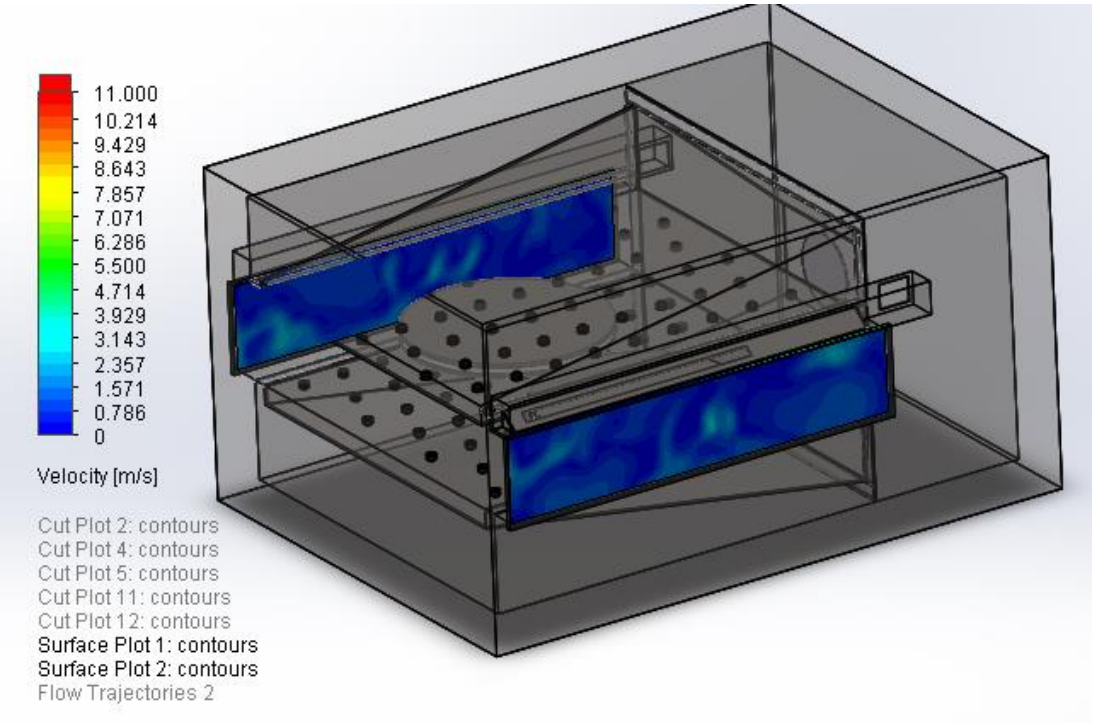

Figure 5.20: Leakage air surface plot

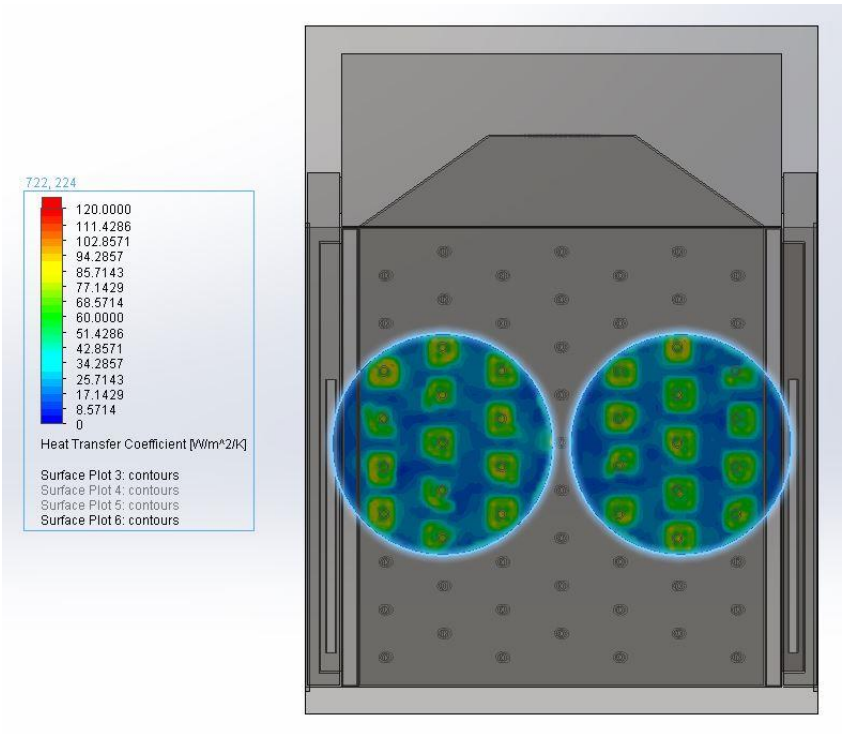

Figure 5.21: Heat transfer coefficient on target surface

Figure 5.20 shows leakage air pattern on left and right open surfaces of the oven for configuration 20. For this configuration, the leakage air introduced into the oven is the least (0.004 lb/s) as compared to all other configurations. Figure 5.21 shows heat transfer coefficient plot on the top surface of the target. Strategically placed impingement holes cover the entire surface area of the target when conveyor is in motion.

5.3 Conclusions

Analysis of key oven parameters shows that a systematic study can be carried out to optimize oven configuration. To obtain necessary air balance between front and back of the oven, tapered finger configuration is necessary. Extruded holes are used so impinging air jets are better directed towards product surface increasing overall heat transfer to the product. As distance between the nozzle and product increases, heat transfer is decreased. For the oven configuration studied in this chapter, H/D ratio of 8 is found to be optimum. For too high or low H/D ratios, the leakage air to ambient increases, reducing the overall efficiency of the oven. For larger S/D ratios, higher separation between neighboring jets causes uneven cooking performance. S/D ratio of 7 is found to be optimal for oven configuration studied in this chapter. Return geometry of the oven can greatly influence leakage air to the ambient thus affecting its efficiency. Higher CFM generally results in high heat transfer but the heating system in the oven needs to be able to support the higher CFM rating of the fan.

CHAPTER 6: CONCLUSIONS AND FUTURE WORK

In this research, a systematic approach is chosen to analyze and optimize controlling parameters of air jet impingement. Single un-bound air jet heat transfer is studied in detail. Many important dependencies are observed. It is shown that highest values of heat transfer coefficient occur at stagnation point. The height of stagnation zone is found to be at a distance D to 1.5D from the impingement surface. Heat transfer coefficient values are optimum for H/D ratios between 6 and 8. Input jet temperature was kept constant for all simulation studies as the trends discussed in this research work are proportional to the input temperature. Varying input temperature does not change the shape of the heat transfer curve over the impingement surface investigated in this study.

Based on the findings from single jet impingement, multi-jet impingement model is built and analyzed. The model is validated against published experimental results. It is observed that high heat transfer coefficient peaks occur at lower H/D ratios but the peaks are more uniform for H/D ratios between 6 and 8. For a fixed velocity, heat transfer coefficient values are directly proportional to nozzle diameter. For a fixed H/D and S/D ratio, heat transfer rate increases as the nozzle velocity increases until it reaches a limiting value. Further increase in nozzle velocity causes drop in heat transfer rate due to ingress of large amounts of cold ambient air into the control volume.

In final chapter a real-world case study of air impingement conveyor oven is investigated. Optimum H/D and S/D ratios found at system level (case study) show close co-relation to the

optimum H/D and S/D ratios found analyzing 3 nozzle arrangement. This shows these intrinsic parameters are scalable to larger systems. When compared to initial configuration, the systematic approach showed improvement in average heat transfer coefficient of 22.7%, improvement in average surface heat flux of 24.7% and improvement in leakage air mass flow rate of 59.1%.

The initial configuration of conveyor oven is designed in a 3D modelling software based on publicly available information and common industry knowledge. For researchers interested in taking this work further, a more complicated transient analysis of entire conveyor oven can be performed. The author has identified high impact key parameters for a conveyor oven. Further work can be done by varying additional parameters as outlined in section 5.2. Based on guidance from this research, a practical approach can be pursued by fabricating a test oven and optimizing its performance.

REFERENCES

[1] Erdogdu, F., Ferrua, M., Singh, S. and Singh R. P. "Air-impingement cooling of boiled eggs: Analysis of flow visualization and heat transfer" Journal of Food Engineering Vol. 79 (2007): pp. 920-928.

[2] Anderson, B. and Singh, R. P. "Effective heat transfer coefficient measurement during air impingement thawing using an inverse method" International Journal of Refrigeration Vol. 29 (2006): pp. 281-293.

[3] Guo, Q., Wen, Z. and Dou, R. "Experimental and numerical study on the transient heat-transfer characteristics of circular air-jet impingement on a flat plate" International Journal of Heat and Mass Transfer Vol. 104 (2017): pp. 1177-1188.

[4] Ansu, U., Godi, S., Pattamatta, A. and Balaji, C. "Experimental investigation of the inlet condition on jet impingement heat transfer using liquid crystal thermography" Experimental Thermal and Fluid Science Vol. 80 (2017): pp. 363-375.

[5] Guoneng, L., Zhihua, X., Youqu, Z., Wenwen, G. and Cong, D. "Experimental study on convective heat transfer from a rectangular flat plate by multiple impinging jets in laminar cross flows" International Journal of Thermal Sciences Vol. 108 (2016): pp. 123-131.

[6] Cafiero, G., Greco, C., Astarita, T. and Discetti, S. "Flow field features of fractal impinging jets at short nozzle to plate distances" Experimental Thermal and Fluid Science Vol. 78 (2016): pp. 334-344.

[7] Zhou, G., Dou, R., Su, F., Liu, S., Li, Z. and Feng, X. "Heat Transfer Characteristics of Cooling High Temperature Steel Plate by Single Round Jet Impingement" Heat Transfer – Asian Research Vol. 44 No. 5 (2015): pp. 410-419.

[8] Wang, B., Lin, D., Xie, Q., Wang, Z. and Wang, G. "Heat transfer characteristics during jet impingement on a high-temperature plate surface" Applied Thermal Engineering Vol. 100 (2016): pp. 902-910.

[9] Ramezanpour, A., Shirvani, H. and Mirzaee, I. "A Numerical Study on the Heat Transfer Charateristics of Two-Dimensional Inclined Impinging Jet" IEEE Electronics Packaging Technology, 5th Conference (2003): pp. 626-632.

[10] Dr Bonis, M. and Ruocco, G. “Modelling local heat and mass transfer in food slabs due to air jet impingement” Journal of Food Engineering Vol. 78 (2007): pp. 230-237.

[11] Dobbertean, M. and Rahman, M. “Numerical analysis of steady state heat transfer for jet impingement on patterned surfaces” Applied Thermal Engineering Vol. 103 (2016): pp. 481-490.

[12] Modak, M., Garg, K., Srinivasan, S. and Sahu, S. “Theoretical and experimental study on heat transfer characteristics of normally impinging two dimensional jets on a hot surface” International Journal of Thermal Sciences Vol. 112 (2017): pp. 174-187.

[13] Marcroft, H. and Karwe, M. “Flow Field in a hot air jet impingement oven - part I: A single impingement jet.” Journal of Food Processing Preservation Vol. 23 No.3 (1999): pp. 217-233.

[14] Banooni, S., Hosseinalipour, S., Mujumdar, A., Taherkhani P. and Bahiraei, M. “Baking of Flat Bread in an Impingement Oven: Modeling and Optimization.” Drying Technology Vol. 27 (2009): pp. 103-112.

[15] Cafiero, G., Castrillo, G., Greco, C. and Astarita, T. “Effect of the grid geometry on the convective heat transfer of impinging jets.” International Journal of Heat and Mass Transfer Vol. 104 (2017): pp. 39-50.

[16] Alamir, M., Witrant, E., Della Valle, G., Rouaud, O., Josset, Ch. And Boillereaux, L. “Estimation of energy saving thanks to a reduced-model-based approach: Example of bread baking by jet impingement” Energy Vol. 53 (2013): pp. 74-82.

[17] Caliskan, S., Baskaya, S. and Calisir, T. “Experimental and numerical investigation of geometry effects on multiple impinging air jets.” International Journal of Heat and Mass Transfer Vol. 75 (2014): pp. 685-703.

[18] Terzis, A. “On the correspondence between flow structures and convective heat transfer augmentation for multiple jet impingement.” Experiments in Fluids Vol. 57 No. 9 (2016): pp. 1-14.

[19] Sarkar, A., Nitin, N., Karwe, M. and Singh, R. P. “Fluid Flow and Heat Transfer in Air Jet Impingement in Food Processing.” Journal of Food Science Vol. 69. No. 4 (2004): pp. 113-122.

[20] Chandramohan, P., Murugesan, S. and Sundaraganesan, A. “Heat Transfer Analysis of Flat Plate Subjected to Multi-Jet Air Impingement using Principal Component analysis and Computational Technique.” Journal of Applied Fluid Mechanics Vol. 10, No. 1 (2017): pp. 293-306.

[21] Garimella, S. and Schroeder, V. “Local Heat Transfer Distributions in Confined Multiple Air Jet Impingement.” Journal of Electronic Packaging Vol. 123 (2001): pp. 165-172.

[22] Penumadu, P. and Rao, A. “Numerical investigations of heat transfer and pressure drop characteristics in multiple jet impingement system.” Applied Thermal Engineering Vol. 110 (2017): pp. 1511-1524.

[23] Kannan, B. T. and Sundararaj, S. “Steady State Jet Impingement Heat Transfer from Axisymmetric Plates with and without Grooves.” Procedia Engineering Vol. 127 (2015): pp. 25-32.

[24] Kocer, D. and Karwe, M. “Thermal Transport in a Multiple Jet Impingement Oven.” Journal of Food Process Engineering Vol. 28 No. 4 (2005): pp. 378–396.

[25] Gardon, R. and Akfirat, J. C. “Heat transfer characteristics of impinging two-dimensional air jets.” J. Heat Transfer Vol. 88 No. 1 (1966): pp. 101–107.

[26] Sarkar, A. and Singh, R. P. “Spatial Variation of Convective Heat Transfer Coefficient in Air Impingement Applications.” Journal of Food Science Vol. 68 No. 3 (2003): pp. 910-916.

[27] Marcroft, H., Chandraseikaran, M. and Karwe, M. “Flow Field in a Hot Air Impingement Oven - Part II: Multiple Impingement Jets.” Journal of Food Processing Preservation Vol. 23 No. 3 (2007): pp. 235-248.

[28] Bejan, A. Convection Heat Transfer, second ed. Wiley, New York (1995).